from the
space science and
engineering center

the university
of wisconsin
madison

SATELLITE MEASUREMENT OF SPECTRAL TURBIDITY AND ALBEDO, AND THEIR RATES OF CHANGE

UWI-SSEC-GAP-71-003

SATELLITE MEASUREMENT OF SPECTRAL TURBIDITY AND ALBEDO, AND THEIR RATES OF CHANGE

BY

Michael McClintock
Alden McLellan
Lawrence A. Sromovsky

A Report to
THE ENVIRONMENTAL PROTECTION AGENCY

On Research Conducted Between
August 1, 1970 and June 1, 1971

Contract No. 68-02-0002

Co-Principal Investigators: Verner E. Suomi and
Michael McClintock

The Space Science and Engineering Center
The University of Wisconsin
1225 West Dayton Street
Madison, Wisconsin 53706

July 30, 1971

CONTENTS

SUMMARY

This report to the Environmental Protection Agency deals with continued research on the feasibility of using satellite-based instruments to study air pollution. The first report in the series was titled "Studies on Techniques for Satellite Surveillance of Global Atmospheric Pollution," and was submitted to the National Air Pollution Control Administration (since incorporated into the Environmental Protection Agency) in September, 1970. Where discussions in the present report depend on the earlier work, an appropriate reference is made[1] rather than repeating the prior material.

The introduction to the present report provides the context in which the report is to be taken. It establishes an overall philosophy for the research program, and therefore provides a logical mechanism for deciding those measurements whose feasibility should be studied, among the many which might be considered purely on technical grounds.

The chapter on regional atmospheric turbidity variations from the ATS-III Satellite carries further the preliminary work which was reported in reference 1.

Analysis of the data presented at that time has been interpreted and correlated with ground level observations made on the same day. Whereas last year no conclusions were possible, we now conclude that air pollution over the Los Angeles basin has indeed been observed on a day when pollution was not particularly bad.

Detection of Aerosols by Near Infrared Scattering examines the possibility of using scattered sunlight in the near infrared spectral region to detect the presence of dust in the atmosphere. It is concluded that this technique is an attractive possibility for quantitative measurements.

The chapter on Sun Glint as an Atmospheric Probe undertakes analysis of several possible experiments. After treatment of the sun glint's usefulness in a generalized way, the possibility of measuring three important aspects of molecular and particulate pollution are examined. We conclude

that the wavelength dependence of atmospheric turbidity due to aerosols can be measured to attractive precision, that the content of certain molecular species, in particular water vapor, can be measured to suitable precision, and that the absolute value of atmospheric turbidity can be obtained without reference to ground stations, although with less, perhaps unsatisfactory, precision.

An appendix, separately available, is a 16 mm film showing the Los Angeles area on 23 April 1968, the day used as data base for the ATS study of air pollution.

I. INTRODUCTION

A working hypothesis of climatologists is that the long-term mean climate of the earth is correlated with the long-term mean temperature near the surface, although recent work of Vonder Haar[2] indicates that other factors are equally or perhaps even more important. Recent concern over the drop in temperature by approximately 0.3°C in the last twenty years is based on this hypothesis. It is thought that a drop of approximately 4° will create climatic conditions that will allow the start of another ice age. However, although linear extrapolation of the recent thirty-year trend has been used to predice ice-age conditions in approximately 240 years, in fact no extrapolation over that period of time is valid without a knowledge of the way in which a change in the long-term mean temperature is related to its causes. Lacking a credible model, linear extrapolation makes no more sense than exponential or oscillatory extrapolation.

In the absence of other perturbing factors, an increase in the carbon dioxide content of the atmosphere would cause a rise in the earth's temperature because of its absorption in the infrared, where the earth's radiation energy is greatest. Particulate matter in the atmosphere could conceivably cause either an increase or a decrease depending on the optical properties of the particles in appropriate regions of the spectrum. Man's activities in technologically sophisticated countries have been increasing both of these constituents, although there is disagreement over whether man or natural causes contribute more particulate matter. The observed temperature decrease has therefore not received a satisfactory explanation.

It cannot be overlooked, of course, that other factors controlling the earth's energy balance may have changed significantly in the meantime, such as the solar constant or the earth's effective emissivity. Measurements of these factors have not been sufficiently precise to note long-term trends. The question of a changing albedo is equally important to a consideration of this problem and must also be taken into account. Recent work of Vonder Haar and Suomi[3] points this up strongly. The most likely thing, of course, is that all the factors are changing, since this is the general rule in real systems, and the observed temperature trends are the result of a combination of causes.

Given the present state of knowledge about the relationship of atmospheric composition to climate, a logical and useful program will address the problem of the earth's radiation energy balance with particular attention to the part played by aerosols and certain molecular constituents, specifically ozone, carbon dioxide and water vapor, since long-term variations in these constituents will affect the radiation balance most profoundly.

Among many things which might be measured, therefore, a need exists for accurate measurements of the aerosol content and its rate of change in the atmosphere. Taken together with other observations, for example, the ground-based network of turbidity measurements in certain locations,[4] these will serve as a guide to the development of the theory needed ultimately to describe the relation between dust and climate change, since any credible theory must be compatible with accurately made measurements.

The relatively simple experiments which the present report deals with could provide a quantitative measurement of global atmospheric turbidity and of its rate of change over long periods. From this information one may obtain directly a knowledge of the amount by which atmospheric aerosols are affecting the earth's energy balance by attenuating both the sun's energy and the radiated energy of the earth itself.

Furthermore, since the measurements could be made in several wavelength intervals, knowledge could be obtained about the effective size distribution of particles in the atmosphere, and how this distribution changes with time. The effect of changing both the quantity and the size distribution of aerosols in the atmosphere could then be extrapolated to provide a part of the needed basis for theories of future climate.

One of the best broadband spectral sources in the visible region of the spectrum is the sun, and this source is particularly useful if one can arrange to calibrate its intensity at each moment a measurement of atmospheric optical properties is made.

The specular reflection of sunlight from the surface of the ocean (the sun glint) is used in an important way in the experiments studied. The primary intention would be to provide a measure of atmospheric turbidity as a function of wavelength.

The effective temperature of the sun is approximately 6000° K, so that the energy radiated to the earth is peaked in the visible region of the electromagnetic spectrum, at about 4850 Å. This is one appropriate region of the spectrum, therefore, in which to measure turbidity of the atmosphere if one is interested in possible climatic effects of suspended particulate matter. On the other hand, the earth radiates most strongly

in the infrared, peaking in the ten micron region of the spectrum. And since much of the suspended particulate matter is in the one-to-ten micron size-range, atmospheric turbidity in this region of the spectrum also is important to questions of the earth's energy balance and climate.

Given that the most important variable quantities in the earth's atmosphere from the standpoint of the planetary radiation balance are probably water vapor, cloud, dust, CO_2 and O_3, it seems important to consider the possibility of measuring these quantities with satellite-based instrumentation. Accordingly, the feasibility of measuring water vapor content of the atmosphere by using the absorption of reflected sunlight from water surfaces at one micron is studied as one of the possible sun glint experiments.

II. REMOTE SENSING OF ATMOSPHERIC POLLUTION VARIATION BY SATELLITE

Upwelling radiation data from the city of Los Angeles as received by the geosynchronous Applications Technology Satellite (ATS)-III at forty-minute intervals on 23 April 1968 is correlated with various ground-based data. The analysis of the data indicates that the atmospheric turbidity decreased throughout this particular day as the upwelling radiation increased. It is implied from the success of this initial step that continuous atmospheric pollution surveillance over global regions from geostationary satellites with the proper instrumentation is indeed an economically realizable goal.

In the past few years a number of scientists from various disciplines have come to believe that the earth's atmospheric mean temperature in this century is directly related to man's induced trends of carbon dioxide content and particulate matter.[5-7] This conclusion concerning particulate loading was obtained from fifty-year data on urban smoke-haze days, turbidity factors from incidence radiation data in Hawaii, and dust-fall in the Caucasus. On the other hand, the thesis has been put forward[8-10] that man's activities have had very little to do with the global increase in dust loading of the atmosphere, but rather that this phenomenon is due to natural processes, such as volcanic activity which has been rapidly increasing over the past quarter of a century.

It has been shown[11] that the absorption and scattering by aerosols of solar radiation along with the reflective properties of the surface underneath determine the albedo of the region. A change in the albedo, which can be caused by a variance in the particulate loading of the atmosphere, results in atmospheric heating and cooling even at surface levels.[12] Small changes in particulate loading or in the type of particulate such that the ratio of absorption to scattering changes can reverse heating or cooling trends.[13]

As a general working equilibrium radiation relationship, we can write[14]

$$(1 - A)S = 4\sigma T^4 \qquad (1)$$

where the left-hand side of Eq. (1) represents the net influx of radiation from the sun. S is the incident solar radiation and A is the earth's albedo consisting of both the albedo of the earth's surface as well as that of the atmosphere above it, σ is the Stefan-Boltzman constant, and T is the radiative temperature of the surface area under consideration. Since the addition of particulate loading or a change in the type of particulate will modify the backscattering and absorption of solar radiation it will, therefore, alter the albedo.

If we let the total albedo A be split up into its two component parts, we have

$$A = A_s + A_a \qquad (2)$$

where A_s is the albedo of the surface and is a function of latitude and longitude. A_a is the albedo of the atmosphere above the surface considered and it is also a function of latitude and longitude except in certain unusual situations such as observations taken near the limb and/or very low sun angles, in which case A_a would depend also on the actual elongated ray paths.

In most situations in which there occurs an increase in pollution or dust, it can correctly be assumed that the backscattering increases also, thereby increasing A_a.[12] However, there are situations which are not uncommon where an increase in pollution or dust will cause a decreasing A_a.[13] Such is the case in this work. A bright area, the city of Los Angeles, which has a relatively high surface albedo, A_s, is observed from above by satellite. Industrial smog, which has a relatively low albedo, A_a, in that it is highly absorbing and has little backscatter, decreases throughout the day of observation in the green channel, where data are available. The upwelling radiation increases during this period.

Computations have been performed[15] showing the effects on global temperature variations due to large increases in aerosol densities. The net effect of increase in particulate density is to reduce the surface temperature of the earth. This is due to the fact that the overall global albedo of the earth's surface is lower than the albedo of the earth covered with some finite amount of an "average kind" of aerosol. From this follows the well-known effect that the intensity of the upwelling radiation increases as the high reflective particulate levels increase. However, as we will see below, this may not be the case in certain situations. If we consider, for example, a region with a large surface albedo such as the downtown section of a large city, a desert, or a snow-covered area over which the atmosphere is polluted with radiation-absorbing industrial particulates, then we can see that in this particular case, unlike the above

situation, the intensity of the upwelling radiation will decrease as the local pollution levels increase.

The computations referred to above[15] show that an increase by only a factor of 4 in global background concentration may be sufficient to reduce the mean surface temperature by as much as 3.5° K. This temperature decrease over the entire globe is believed to be sufficient to trigger an ice age. However, this argument rests upon increasing the rate of temperature decrease with increasing aerosol loading due to the exponential backscattering of particulates whose minimum single scattering albedo was arbitrarily chosen to be .90. This value, which is low for present day global mean aerosols, implies that the absorption and backscatter fractions with the visible range of wavelength are equal. But, in fact, industrial particulates, which are increasing globally at a much higher rate than natural particulates,[5-7] have a much lower single scattering albedo. Thus, if present trends continue until industrial aerosols contribute a large percentage of the total global scattering centers, then the mean aerosol absorption will increase, giving a much lower value for the single scattering albedo, thereby reversing the influence of atmospheric particulate loading from that of lowering the surface temperature of the earth to that of increasing the temperature of the earth. This could enhance the heating effect due to atmospheric carbon dioxide and possibly cause rapid global climate change.

The feasibility study begun last year to investigate the possibility of monitoring the variation in turbidity over a regional area by means of passive remote sensing from a satellite in earth-synchronous orbit was continued. Our work to date has shown that the relative change in sun-reflected radiation over the city of Los Angeles, California on 23 April 1968 as measured by the green channel data from the geostationary Applications Technology Satellite III, located 35,000 kilometers from earth, can be successfully correlated with ground-based data, such as local horizontal visibilities and reflectometer measurements of sampled particulate matter.

Following the initial analysis reported last year,[1] additional ground-based data were obtained for correlation with satellite observation of the Los Angeles basin on 23 April 1968. The data indicate that the haze growth over Los Angeles decreased throughout the day under study, if this is the proper interpretation of an increase in the relative reflected radiance as received by satellite after sun angle effects have been accounted for. This interpretation is indeed borne out by surface observations of particulate

matter visibility-ranges within the urban area, as well as individual molecular components of atmospheric pollution such as carbon monoxide, nitric oxide, and nitrogen dioxide.

This feasibility program in detecting local atmospheric pollution over cloud-free urban areas was constructed by reducing and analyzing radiance data from the Multicolor Spin Scan Cloud Camera (MSSCC) aboard the Applications Technology Satellite III (ATS-III). The ATS-III satellite is in synchronous earth orbit at 35,000 kilometers height, and on 23 April 1968, its subsatellite point was located at the equator and 60 degrees west longitude. The Multicolor Spin Scan Camera on board the ATS-III consists of a high-resolution telescope, three photomultiplier light detectors, and a precision latitude step mechanism, which when combined with the spinning motion of the ATS-III satellite (100 rpm), permits scanning a complete earth disc. Computer programs and other data reduction procedures were set up in order to correlate statistically, sample, and average high-resolution radiance values throughout a single day over three nearby cloud-free regions of different brightness levels. These three regions were: water (a 60 × 60 km area in the Pacific Ocean off the Baja peninsula), city (the Los Angeles city area), and desert (a relatively flat region in the Altar Desert). (See Figures 1 and 2.) The day of 23 April 1968, a cloud-free day over the three regions under study, was chosen as the day for analysis. Nine digital raw-data tapes of the green channel from the MSSCC system at forty-minute intervals throughout this day were available for study at the Space Science and Engineering Center at the University of Wisconsin. It was found that the radiance over the ocean, over the Los Angeles area, as well as over the Altar Desert decreased throughout the day. However, assuming that haze over the water and the haze over the desert did not change during the day, it can be shown that in these two cases the radiance decrease, which is due to sun angle variation, may be used to account for the sun angle variation of the radiance decrease over the Los Angeles area. The result is that the relative radiance over the Los Angeles area increased, implying that the turbidity decreased during the day. This result, discussed in terms of the local horizontal visibility, particulate matter, and local weather conditions, implies in a straightforward manner, a method of monitoring global atmospheric turbidity as well as local turbidity by means of geosynchronous satellites. It is also clear that with the appropriate sensing detectors on board satellites, the possibility of continuous monitoring of the time and spatial profiles of atmospheric molecular pollutants as well as particulate matter can be achieved over cloud-free areas.

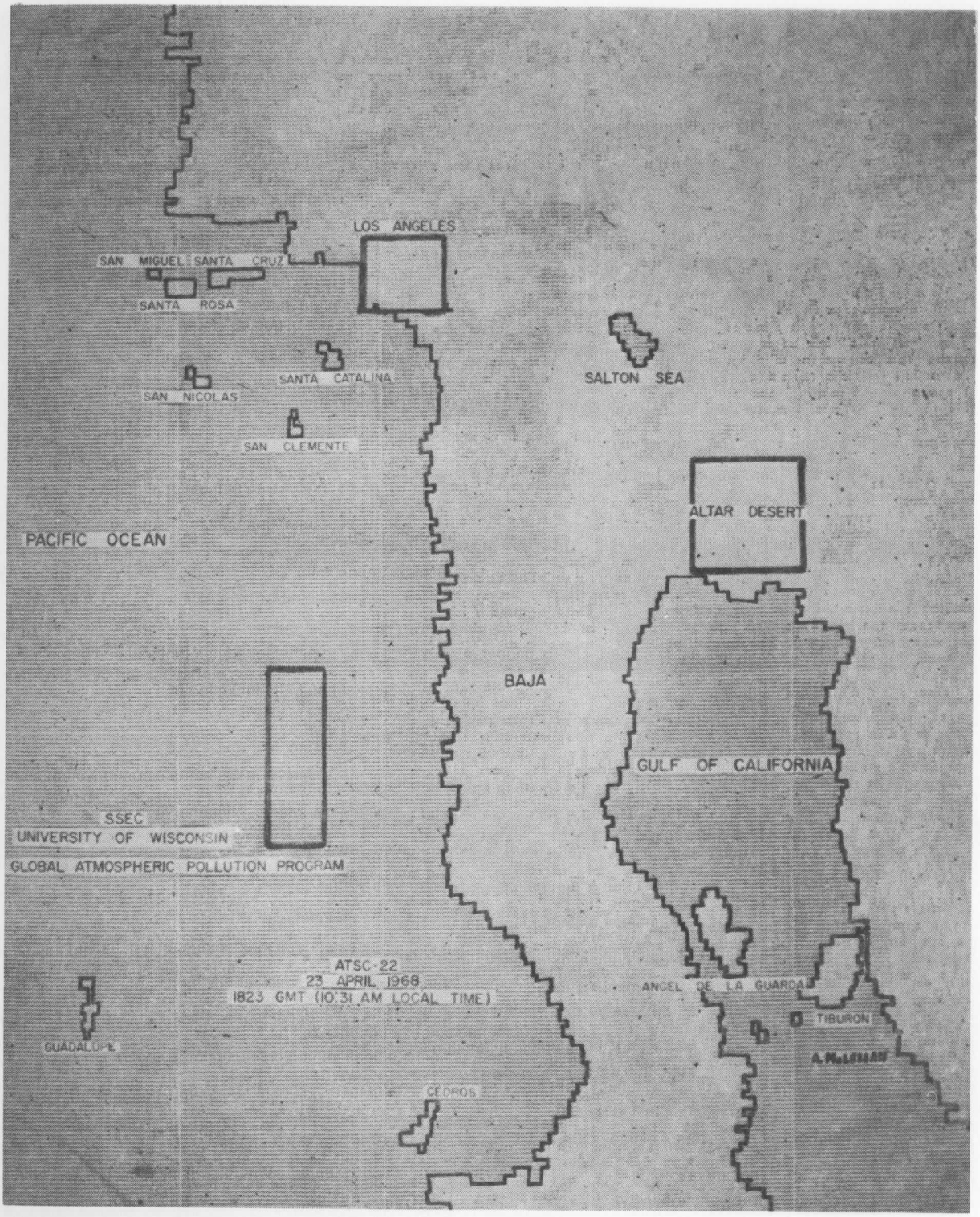

Figure 1. Data display modified by shading for navigation purposes.

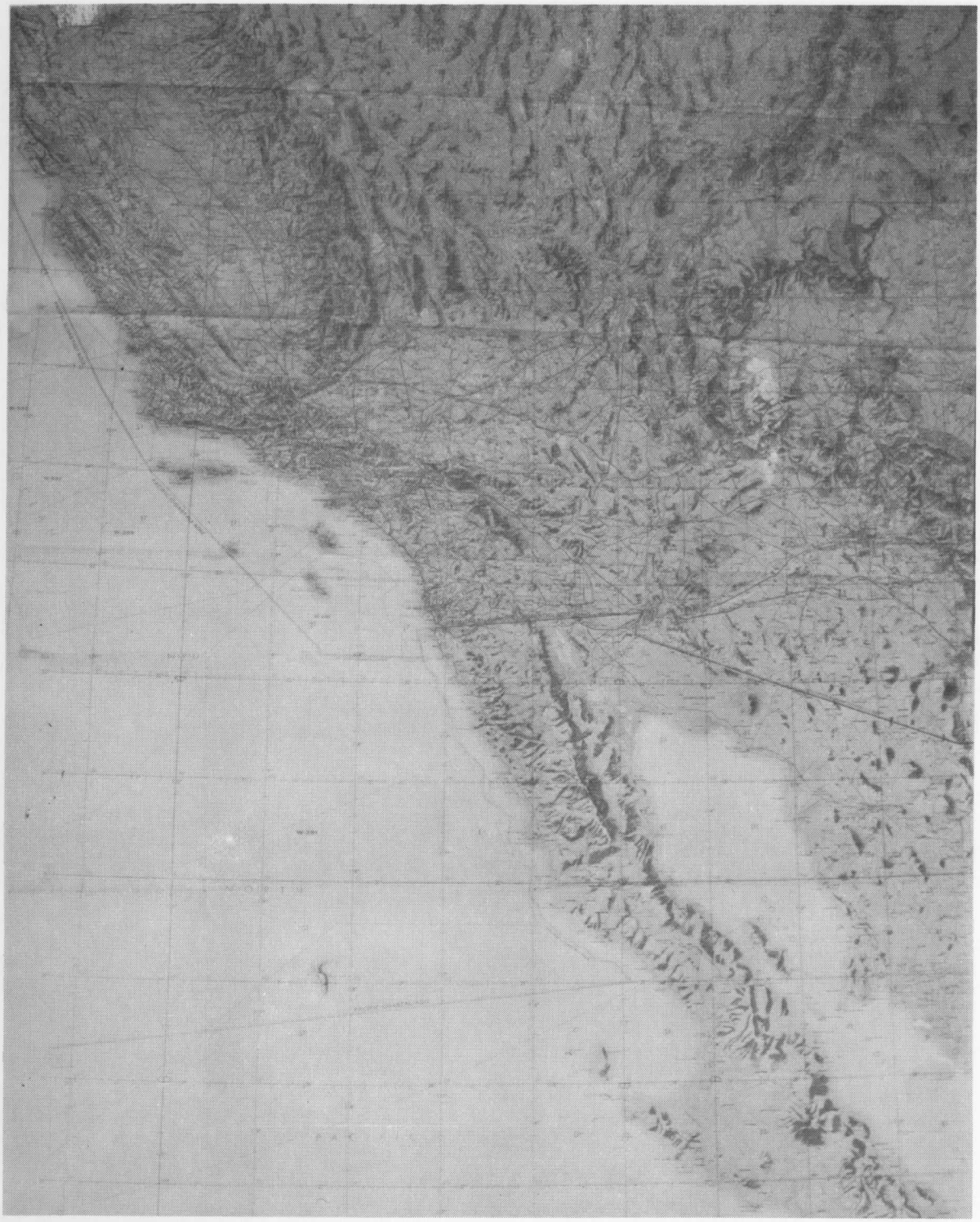

Figure 2. A geographical map of the region for comparison with the foreshortened digital satellite display

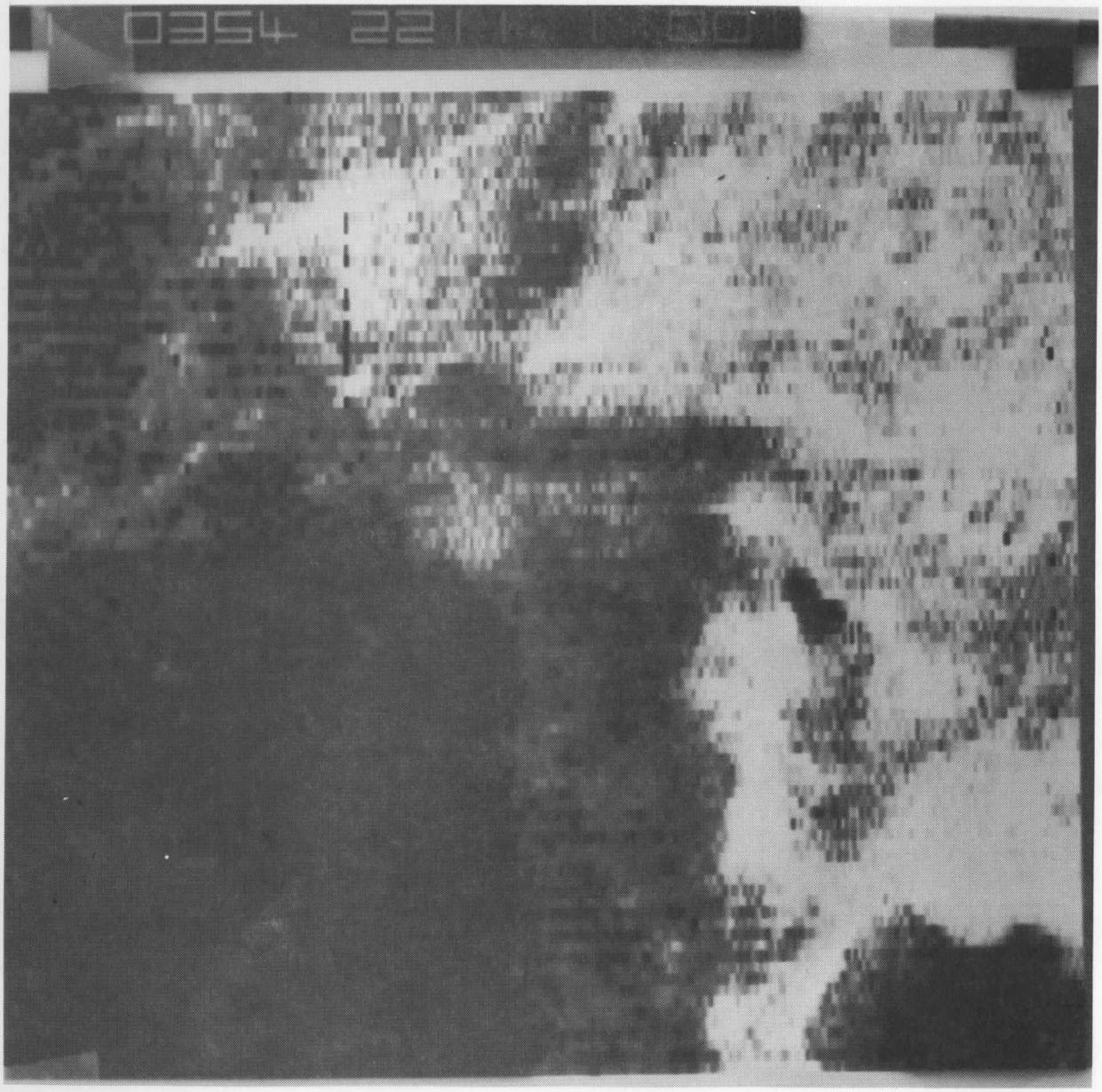

Figure 3. 10:24 AM PST

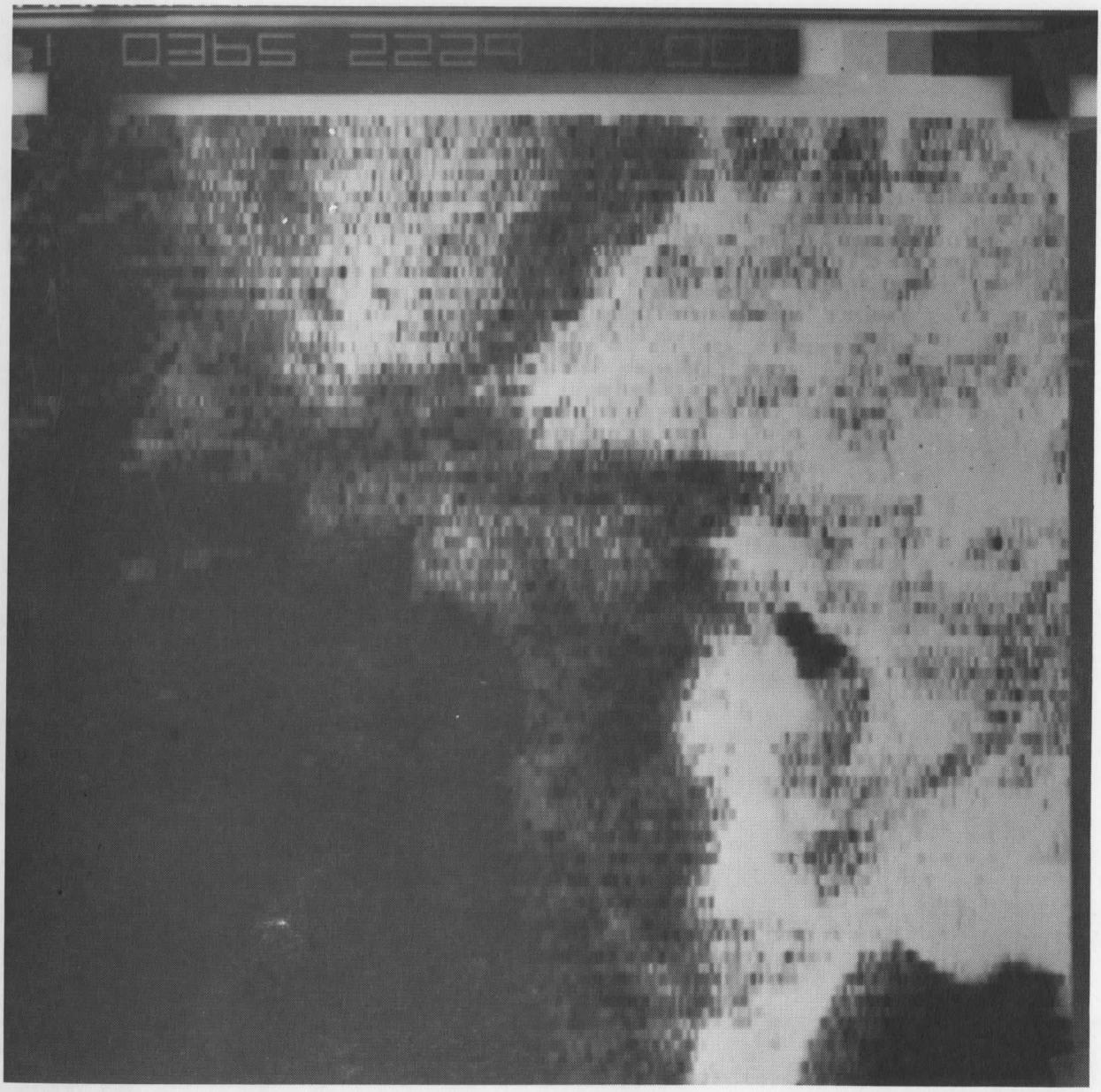

Figure 4. 12:30 PM PST

Results

The two computer photographs, Figures 3 and 4, are images of the southern California area during the day of 23 April 1968. The data were modified by special computer techniques to enhance the coastline and eliminate the effect of the changing position of the sun. The Salton Sea can be seen as a small dark area to the right of center. The city of Los Angeles is a relatively bright area to the left of the Salton Sea and on the coast. Note that the brightness of Los Angeles relative to its surroundings increases during the hours for which satellite pictures were made. As shown in the final graph, Figure 7, this correlates with the decreasing atmospheric pollution over Los Angeles.

Hourly values of the reflected earth radiance as seen from ATS-III satellite from the Altar Desert (top curve), the city of Los Angeles (middle curve), and an area in the Pacific Ocean near Baja (bottom curve) is shown in Figure 5. Each data bar contains a number of data points which are radiance averages taken over a series of smaller areas. The line connecting the data bars is drawn through the points to which the radiance values converged as successively smaller areas were chosen.

Figure 6 presents the hourly variation of three major molecular pollutants within Los Angeles. These data for carbon monoxide, nitric oxide, and nitrogen dioxide, obtained from the Los Angeles County Air Pollution Control District, show in each case the drop-off in concentration for the hours 0800-1600 PST. Note also that the major variation in each concentration occurred in the morning hours, which concurs with the variation in particulate matter and visibilities as shown in Figure 7. Carbon monoxide does not play a role in the formation of particulate matter, and it should have no direct relationship to the variation in upwelling radiation at .55μ.

Data are presented in Table 1 of Ref. 1 showing the corrected radiance values for the Los Angeles region as well as the ground-based hourly data of horizontal visibility and sampling of particulate matter. The visibility data, determined from the sighting of landmarks, refer to horizontal visibility observations rather than vertical observations. Also, these ground-based visibility data cover a broader bandwidth (the visible spectrum) than the green channel ATS data. The particulate matter observations are an indication of the amount of smoke, soot, and tarry matter in the atmosphere. By means of a Chaney Auto-Sampler, a filter sample was taken hourly and the albedo of the deposit was measured using a reflectometer. Therefore, these data give an indication of the amount of pollutant material available in the atmosphere for the absorption of visible radiation. The unit of measurement, K_m, is defined as the deposit which produces an absorbance of 0.1 when the deposit area is one square centimeter and the volume of air sampled is one cubic meter. These data are graphed in Figure 7.

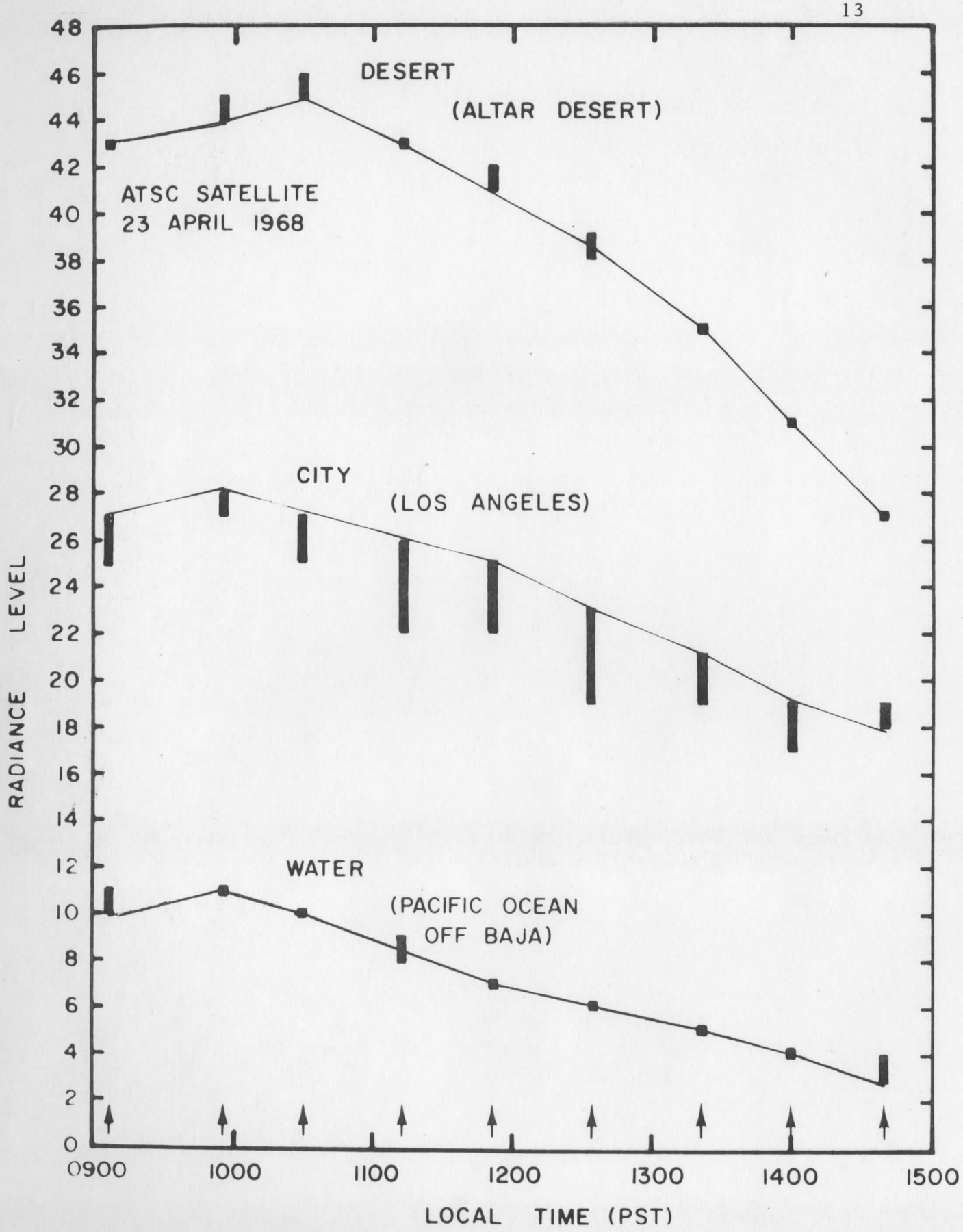

Figure 5. Reflected earth radiance on 23 April 1968 from the Altar Desert (top curve), the city of Los Angeles (middle curve) and an area in the Pacific Ocean near Baja (bottom curve). The decrease in radiation throughout the day for all curves is predominantly due to the changing satellite-sun angle.

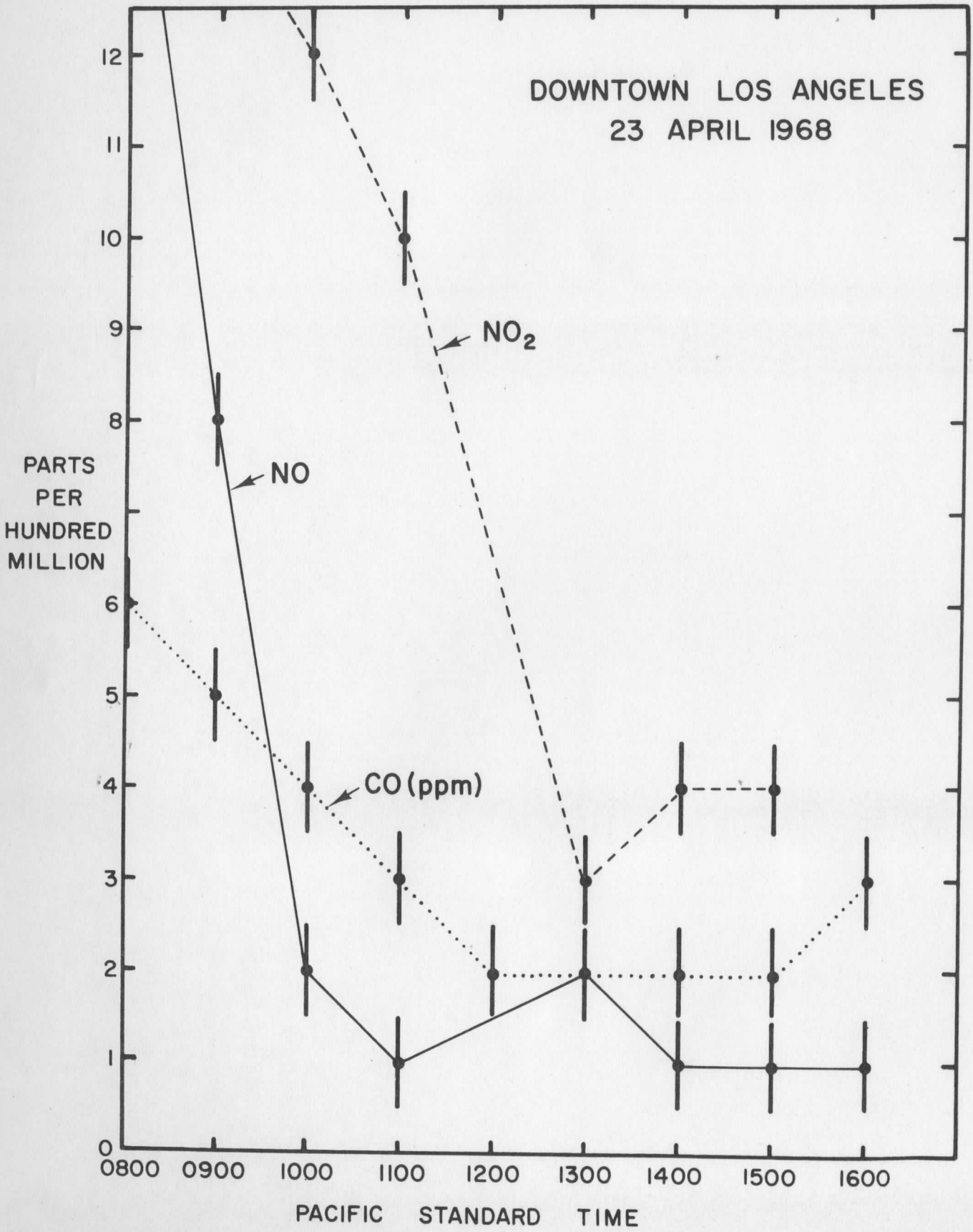

Figure 6. The hourly variation of three major molecular pollutants within Los Angeles on 23 April 1968. The concentration of carbon monoxide nitric oxide, and nitrogen dioxide fell off most quickly during the morning hours.

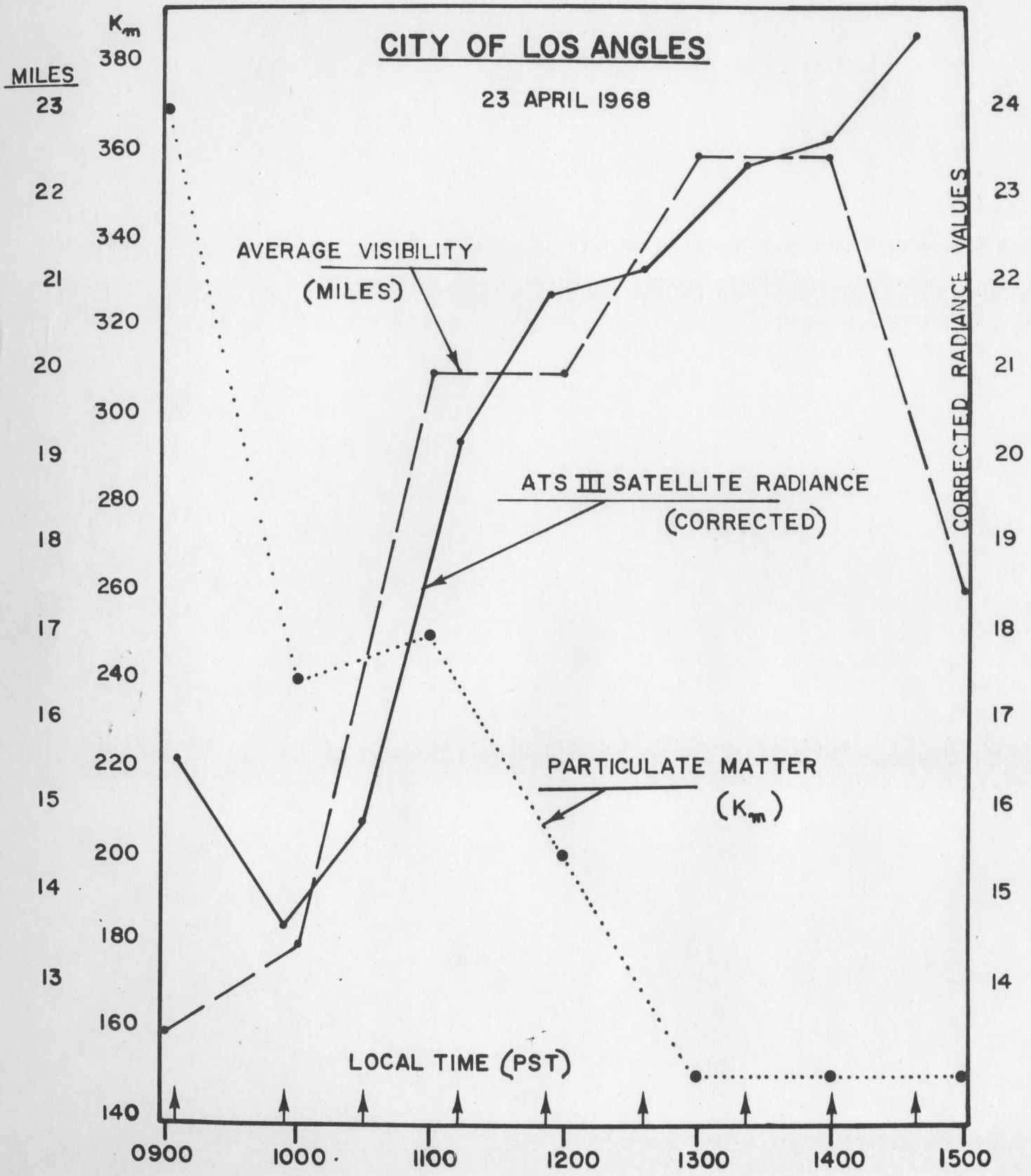

Figure 7. Ground-based data of visibility and of measurements of particulate matter confirm the ATS radiance data that the atmosphere's turbidity over Los Angeles decreased during the day of 23 April 1968.

Conclusions

From Figure 7, we see that the ground-based data confirm the interpretation of the ATS data, which is that the atmospheric turbidity, or at least that component of the atmosphere over Los Angeles which is optically absorbing, decreased from 0900 to 1400 PCT on 23 April 1968. The local climatological data of ESSA's Environmental Data Service for the International Airport in Los Angeles and the Municipal Airport in Long Beach indicates that westerly winds increased from two to sixteen knots in the late afternoon, that the horizontal visibility increased and reached a maximum in the late afternoon, and that cloud-cover, consisting of thin cirrus wisps increased from zero suddenly to 8/10 at 1600 PCT. It is to be noted that throughout the entire day unlimited ceiling was reported; therefore at this time no correction for "cloud noise" has been made, since most of the satellite data was taken during the morning and early afternoon hours. In any case, the interpretation of the relationship between satellite and ground-based data during the last hour in Figure 7 is to be done with caution.

It is implied from the success of this initial step that continuous atmospheric particulate matter surveillance over local areas from geostationary satellites is indeed a realizable goal.

III. DETECTION OF AEROSOLS BY NEAR-INFRARED SCATTERING

Introduction

The scattered solar radiation leaving the earth's atmosphere ultimately results from three distinct phenomena (omitting clouds from the discussion): 1) scattering by atmospheric molecules (Rayleigh and Raman scattering, and resonance absorption followed by re-emission), 2) Mie scattering by atmospheric aerosols, and 3) scattering (or reflection) by the earth's surface. We include the possibility that the scattering is inelastic, i.e., that absorption is present. These three processes interact with each other and generally cannot be treated by means of linear superposition. Specifically, any attempt to infer from satellite radiance measurements the properties or even the presence of atmospheric aerosols must deal with the scattering properties of the earth's surface and with the nonlinearities of multiple scattering. These difficulties are particularly troublesome at wavelengths for which the atmosphere is optically thick, i.e. the visible region of the spectrum, and become less so at wavelengths for which the atmosphere is optically thin, i.e., the near-infrared spectral region. We shall attempt to demonstrate here the advantages that can be gained by using the near-infrared scattering from aerosols for their detection and measurement.

Scattering Properties of Aerosols

Aerosol particles have dimensions comparable to the wavelength of visible light, and are thus Mie scatterers. The precise scattering properties of a given aerosol depend upon the composition of the individual particles, their distribution of sizes, and their total number. All of these factors can vary enormously from one time or place to the next.[16] Certain general characteristics can be described, however, especially the major contrasts with Rayleigh scattering.

As indicated in Figure 8, the typical aerosol scattering phase function is very large in the forward direction (accounting for the brilliance of the sun's aureole, for example), and is relatively small in the backward direction. This latter factor adds considerably to the difficulty of directly

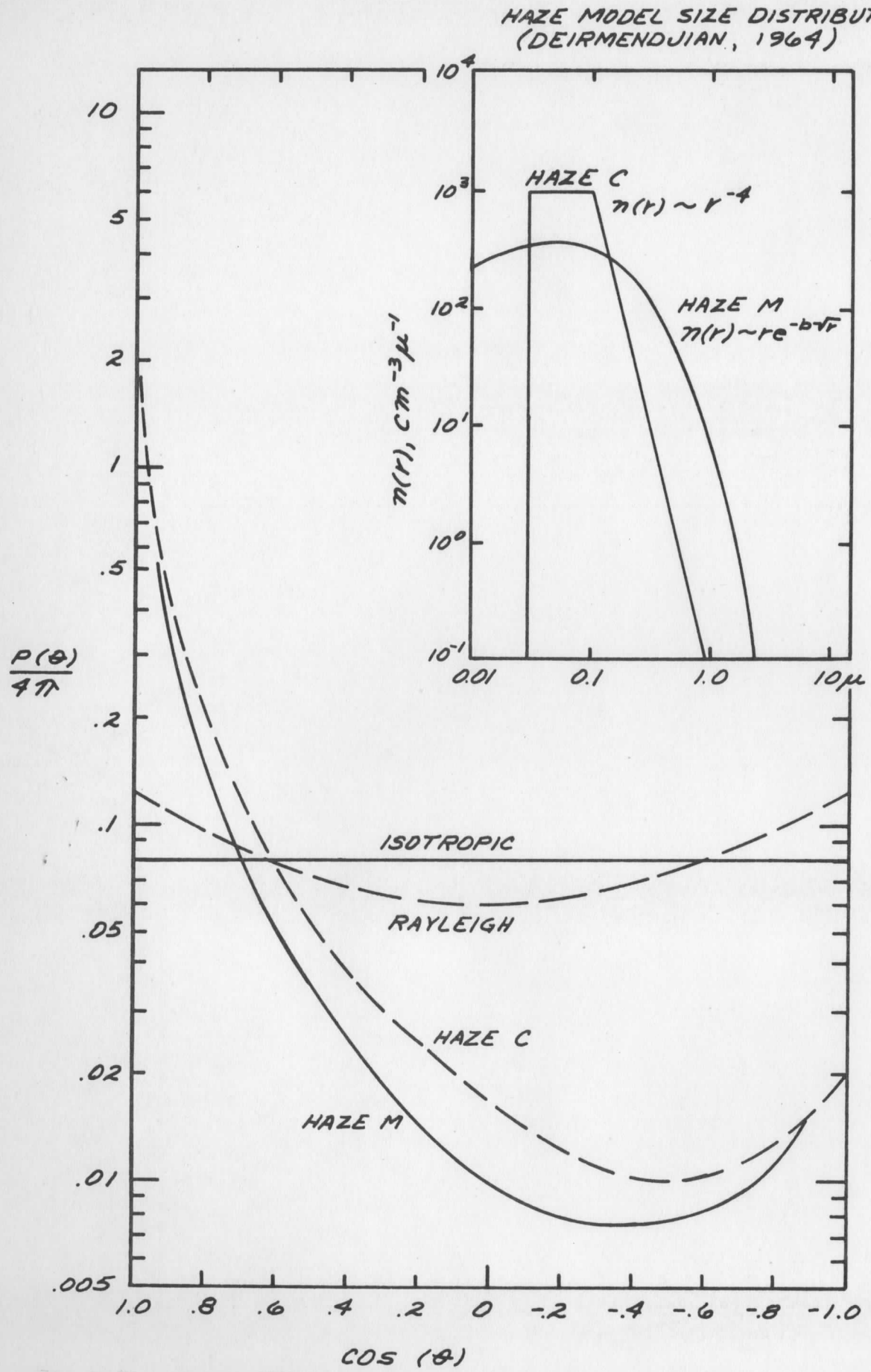

Figure 8. Aerosol and Rayleigh phase functions (from Kattawar and Plass, 1968). Haze models C and M (Deirmendjian, 1964) approximate the size distributions for continental and maritime haze, respectively.

observing aerosol scattering from a satellite platform. For the same optical thickness, Rayleigh scattering at 0.7 microns is ten times as large as aerosol scattering in the backward direction.

In spite of the backscattering inefficiency of aerosols, they can become dominant at long wavelengths because the aerosol optical depth for a given concentration does not fall off with increasing wavelength as rapidly as the Rayleigh optical depth. As shown in Figure 9, aerosol extinction falls off much more slowly than the λ^{-4} rate characteristic of Rayleigh scatterers. Thus, by observing in the near-infrared, the percentage effect of aerosols on atmospheric radiance can be dramatically increased.

An important factor which is not well-specified by the aerosol models we have been considering is the inelastic nature of aerosol scattering. Part of the radiant flux passing through an aerosol may be converted into another form of energy instead of merely being scattered in a different direction. This nonconservative component, which depends on the composition of the aerosol particles, is important in determining whether increasing aerosol loading results in increased radiance or decreased radiance. Recent papers by Atwater[11] and by Rasool and Schneider[15] demonstrate that the sign of the albedo change depends upon the ratio of backscattering to absorption, and upon the surface albedo. Also significant in this connection is the vertical distribution of aerosols. As shown in Figure 10, aerosols are concentrated near the bottom of the atmosphere. This factor, in combination with a thick Rayleigh atmosphere, significantly reduces the amount of aerosol scattering visible from above the atmosphere.

Simple Interactions

In order to obtain some intuitive feeling for the interaction of Rayleigh, aerosol, and surface scattering, we shall consider some highly idealized examples. Figure 11 depicts a Rayleigh atmosphere, an aerosol layer, and a surface in different configurations.

Assuming a unit incident solar flux density, the scattered radiances are given by the scattering coefficients S_R, S_A, and S_S, where R, A, and S refer to Rayleigh, aerosol, and surface components, respectively. The primed coefficients are used to indicate additional modifications due to multiple scattering in addition to those resulting from direct scattering and attenuation. To describe attenuation we use the optical depths τ_R and τ_A for Rayleigh and aerosol components, respectively. It should be noted that the breakdown of total scattering into components is not justifiable in the case of strong multiple scattering. Nevertheless the procedure is useful in estimating the qualitative effects of aerosols.

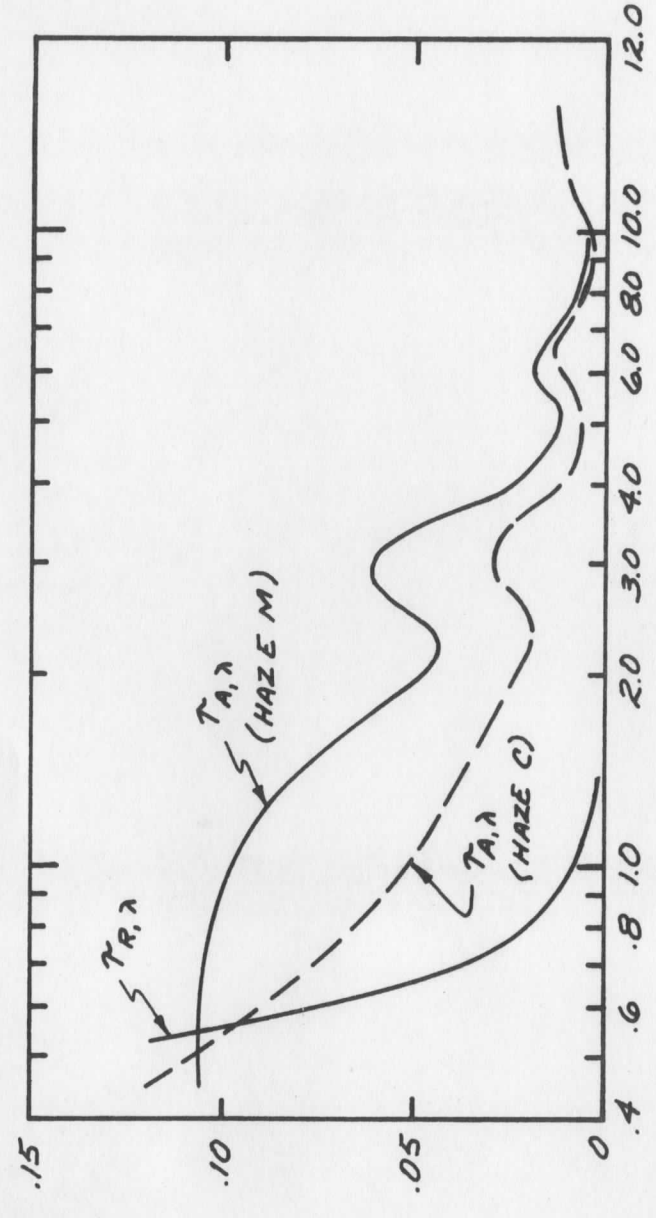

Figure 9. Aerosol and Rayleigh extinction coefficients as a function of wavelength (Deirmendjian, 1964). Haze C and Haze M are as in Figure 8.

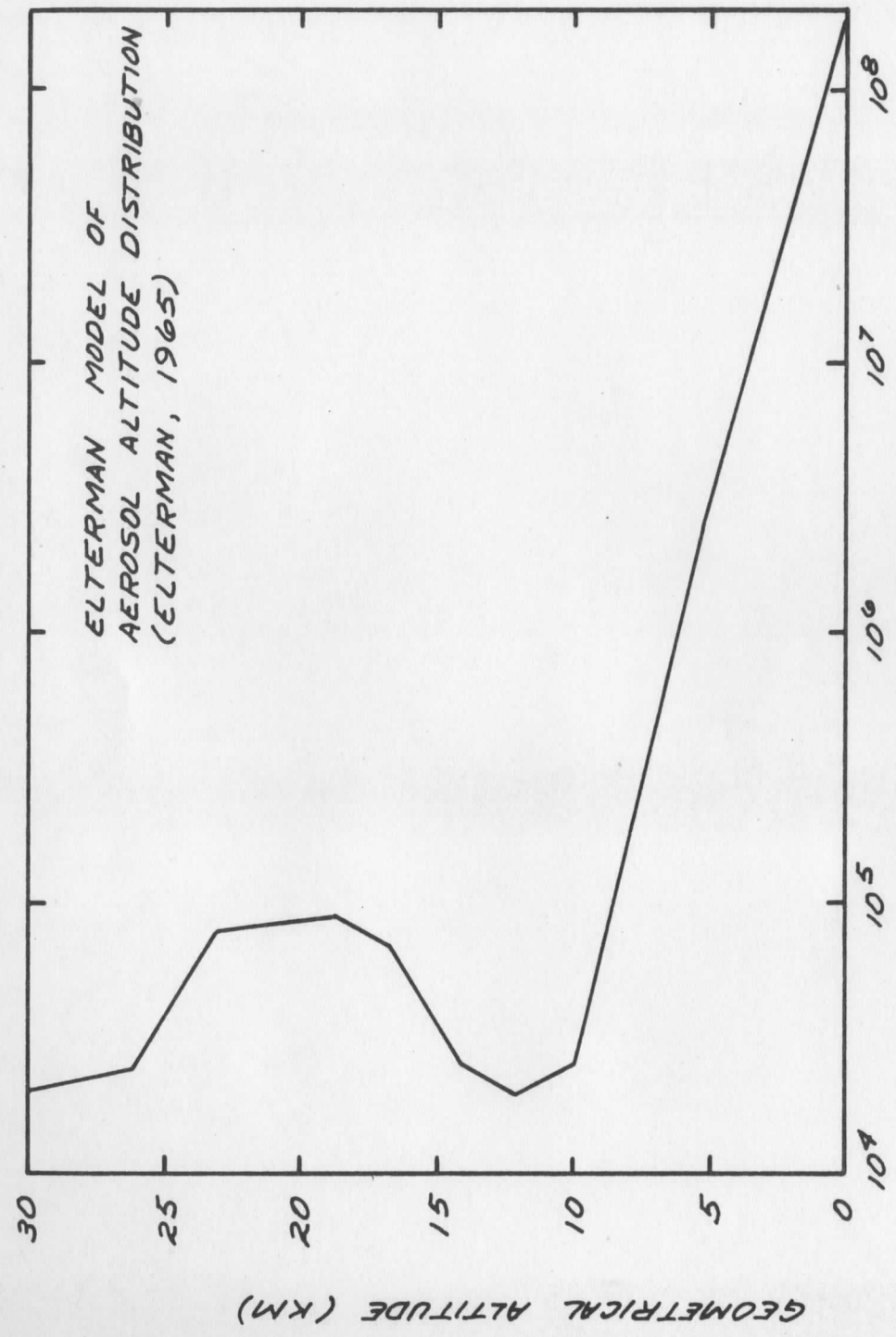

Figure 10. Elterman's model of the vertical distribution of aerosols.

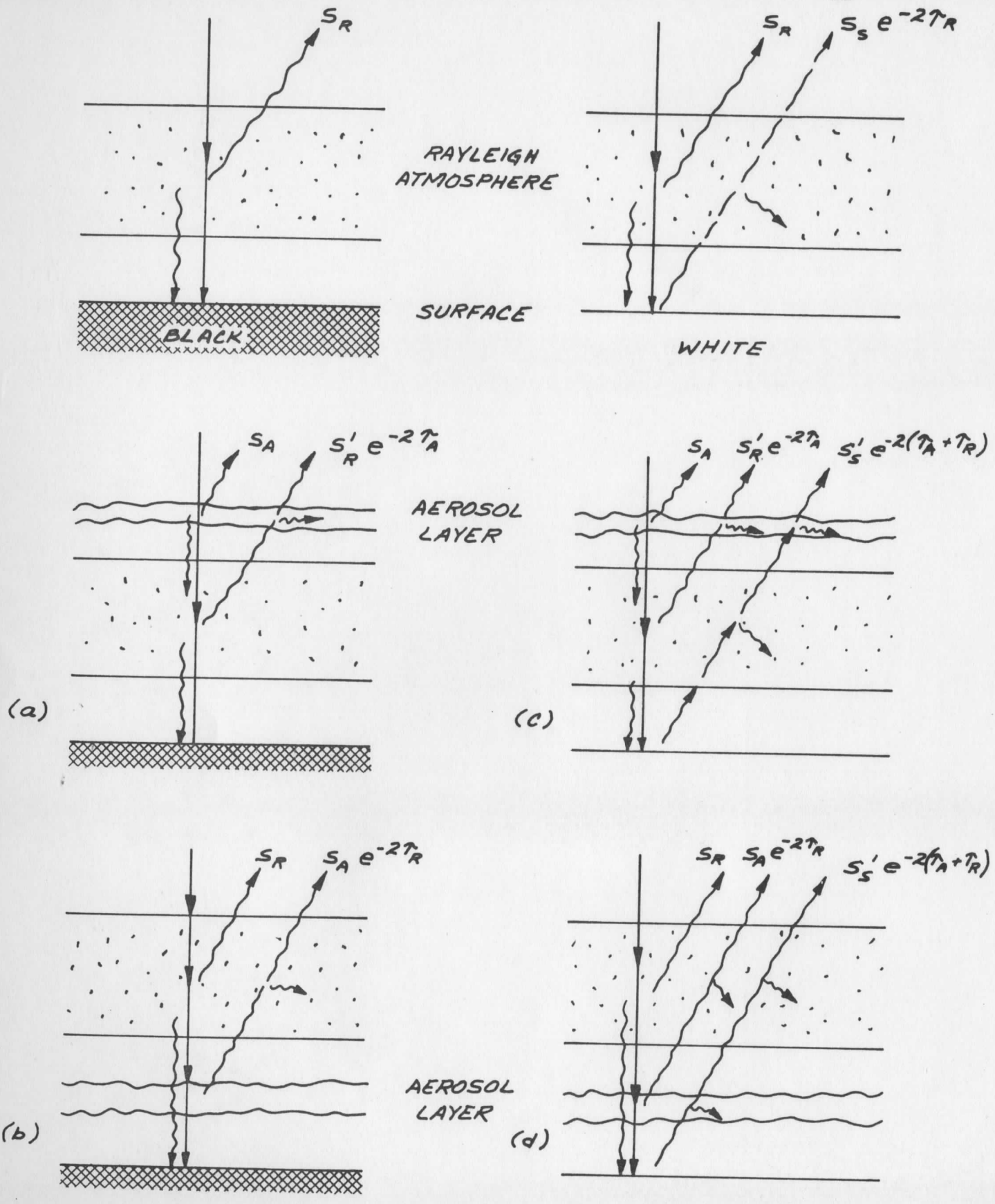

Figure 11. Diagrams for estimating the effect of aerosols on scattered radiances.

In cases (a) and (b) the surface is black (all incident flux is absorbed). Adding an aerosol layer at the bottom of the atmosphere clearly results in increased radiance, since part of the originally absorbed radiation is scattered back (approximately given by $S_A e^{-2\tau_R}$). If the aerosol is above the atmosphere, as in case (a), the results can be quite different. The flux incident on the Rayleigh atmosphere is reduced by a factor $e^{-\tau_A}$, leading to a corresponding reduction of the Rayleigh scattered component. Since part of the flux attenuated by the aerosol layer is scattered into the Rayleigh atmosphere a slight increase from $S_R e^{-2\tau_A}$ to $S'_R e^{-2\tau_A}$ will result. This cannot make up for the attenuation factor because at least some of the attenuated fraction is absorbed by the surface and by the aerosol. Given the relatively small size of S_A it is quite probable that the increase due to this contribution will not be enough to offset the decrease. The result would be a reduction in apparent radiance. For a realistic aerosol distributed within the atmosphere, either an increase or a decrease (or neither) might be possible. In view of Figure 10, an increased radiance above a black surface appears most likely.

For a surface of very high albedo (cases (c) and (d)) and a partially absorbing aerosol, a reduction of radiance would result from an increase in aerosol content. This is true no matter how the aerosol is distributed in the atmosphere, since part of the incident flux is lost from the radiation field. For a surface of intermediate albedo, an estimation of the effect of aerosols can be exceedingly complicated if the atmosphere is optically thick. Only multiple scattering calculations including absorption can produce reliable results. It is clear even from this crude analysis that there exists a surface albedo which makes the aerosol appear invisible. That is, by introducing an aerosol into the atmosphere above the surface specified, no change of radiance is observed. With certain simplifying assumptions, Atwater was able to determine for a given surface albedo an equilibrium value of the absorption to backscattering ratio for which the albedo change with aerosol increase is zero.[11]

Tentative Conclusions

Our initial discussion thus indicates a high degree of ambiguity in the interpretation of satellite-observed radiance in terms of aerosol content or properties. Probably the ideal situation for aerosol measurement from satellites would be over accurately calibrated surfaces of high albedo and very low albedo, for wavelengths at which Rayleigh scattering is negligible. This would make possible a determination of two important aerosol effects: the absorption of radiation, measurable as a reduction in albedo of high-

albedo surfaces; and the backscattering of radiation, measurable as an increase in albedo over a nearly black surface. In the near-infrared, the sea surface is very black (away from regions of sun glint and high seas). Thus, increasing aerosol over the sea surface should be clearly seen as increasing spectral radiance. Although high-albedo land areas are also apparent at near-infrared wavelengths, calibrating such surfaces accurately enough to detect the small radiance changes due to variations in absorption by aerosols may prove to be exceedingly difficult. These conclusions are also supported by the multiple-scattering calculations of Kattawar and Plass.[17]

Multiple-Scattering Results

In a recent paper[18] a Monte Carlo method is applied to the multiple scattering in a realistic model of the earth's atmosphere, including an inhomogeneous distribution of aerosols. The aerosols used by the authors are represented by particles with a real index of refraction of 1.55 and a size distribution corresponding to the Haze C model proposed by Deirmendjian[19]. Results for radiance leaving the atmosphere are presented for albedos of zero and one, wavelengths of .4μ and .7μ, and for aerosol amounts one-third normal, normal, and three times normal. Here normal is taken to be the amount specified by Elterman[20] in the Handbook of Geophysics and Space Environments. At .4μ and zero albedo, increasing aerosol amount shows increasing radiance (Figure 12). No definite trend is observable for an albedo of unity. Although the magnitude of the radiance is much larger in this case, the effect of aerosols is much smaller, especially in terms of percentage effects. The increase observed over a zero albedo surface is in agreement with our previous discussion.

At a wavelength of .7μ (Figure 13), the Rayleigh atmosphere is considerably thinner and the difference between the two cases is considerably larger than at .4μ. In this case (for A = 0), introducing the normal amount of aerosols doubles the observed radiance. Thus, even at the modestly increased wavelength of .7μ, aerosols over a black surface have a dominant influence on the observed radiance conclusions.

Conclusions

The Plass and Kattawar results are unrealistic to the degree that they do not account for the possible nonconservative scattering of aerosols. This would show up as a reduction in radiance over a surface of unit albedo, as we have seen, and this reduction might be a sensitive measure of aerosol content. Nevertheless, some conclusions can be drawn from the results which are not altered by this deficiency. These are:

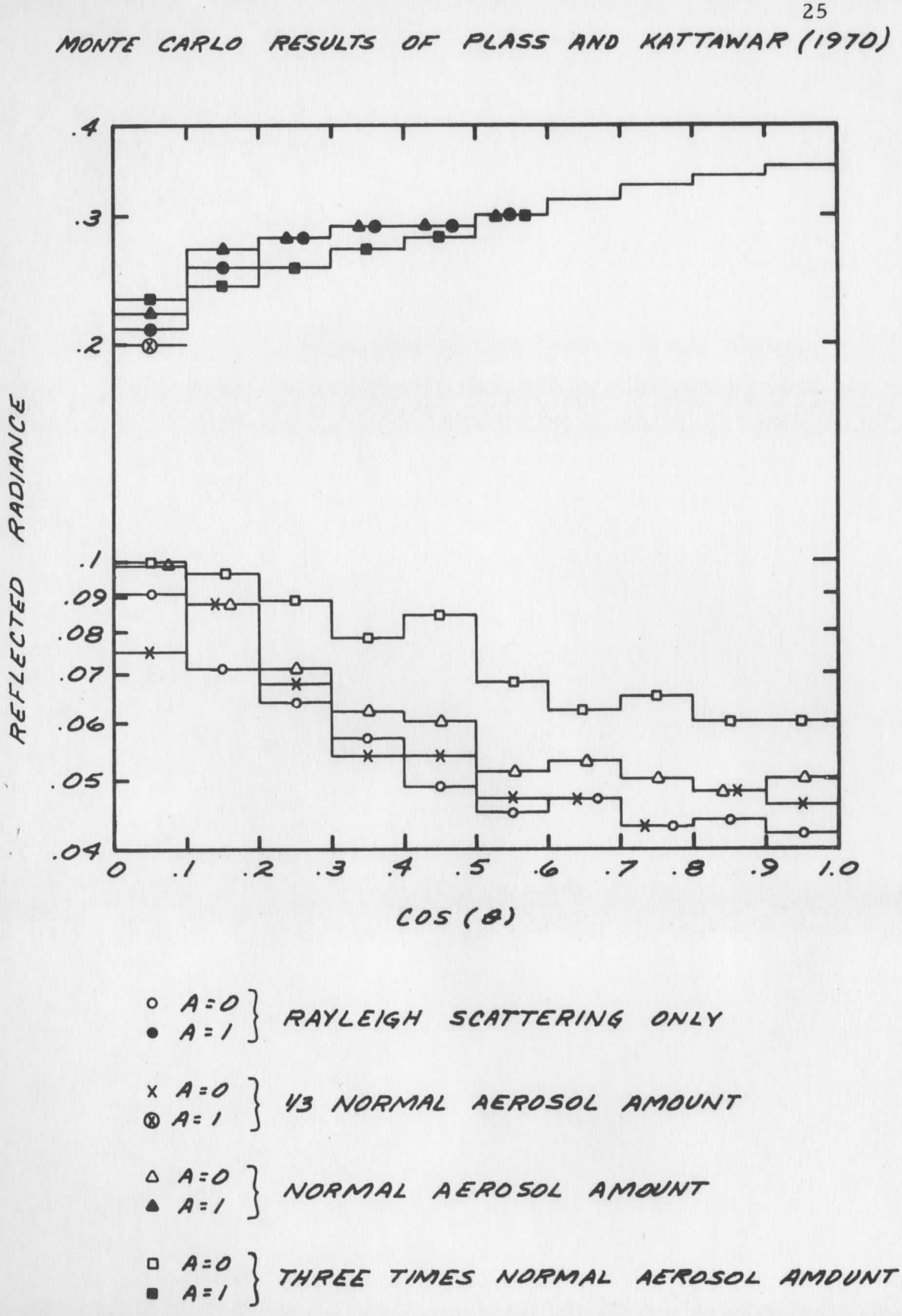

Figure 12. Reflected radiance for $\lambda = .4\mu$, sun at the zenith, observer at zenith angle of cosine θ (Plass and Kattawar, 1970).

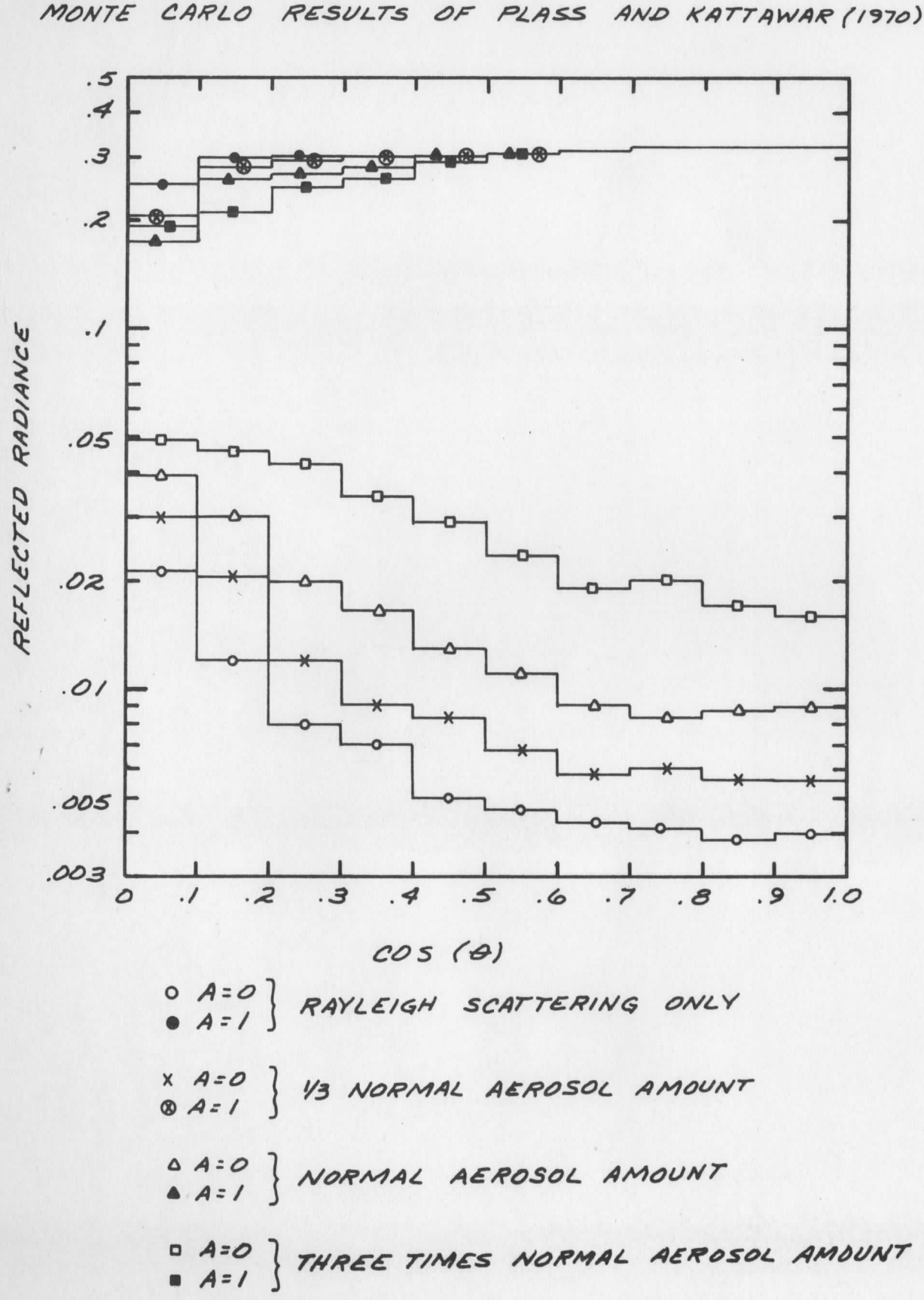

Figure 13. Reflected radiance for $\lambda = .7\mu$, sun at zenith, observer at zenith angle of cosine θ (Plass and Kattawar, 1970).

(1) Aerosol effects on scattered radiance are most easily observed when Rayleigh scattering is small.

(2) Unambiguous interpretation of radiance effects by aerosols requires a calibrated surface. (The most readily available calibrated surface in certain regions of wavelength is the surface of the sea.)

(3) The best observing conditions for detection of aerosols are obtained in a near-infrared window over a black surface.

We have made some preliminary investigations with existing satellite data, but have found it inadequate for a demonstration of the feasibility of near-infrared aerosol measurements. Red Channel data from ATS-III was studied in an attempt to use deviations from the Rayleigh angular distribution to detect aerosols (following a suggestion by Suomi). However, digitizing noise in the red channel data was too severe to allow its use for this purpose. In addition, from Figure 13 (Plass and Kattawar results), we see that, even without digitizing noise, the fact that variations of the angular distributions with increasing aerosol content are quite small, compared to total radiance variations, would have seriously complicated the attempt to use uncalibrated radiances for this purpose. It seems quite clear that calibrated radiances at near-infrared wavelengths will provide the most sensitive measure of aerosol loading from satellite observations.

Our final conclusion is that the satellite measurements of aerosols in the near infrared is an attractive possibility and should be undertaken if more detailed calculations continue to bear out the feasibility.

IV. SUN GLINT AS AN ATMOSPHERIC PROBE

Introduction

Surface-based measurements of the attenuation of solar radiation by the atmosphere have revealed a wealth of information about its molecular and particulate constituents. It would be desirable to make such transmission measurements from a satellite platform in order to sample larger atmospheric volumes than is possible from the surface, and also in order to sample regions of the earth poorly covered by surface sensors (e.g., the oceanic regions). In addition, satellite observations might make possible the tracking of some variable constituents on a global scale.

It has been proposed that the sun glint (reflection of sunlight from the sea surface), which is so prominent in pictures from the ATS and many other satellites, could be used to determine both the absolute magnitude and relative wavelength dependence of atmospheric transmission over much of the wavelength region between .4μ and 4μ. In essence the sea surface is treated as a mirror of imperfect but determinable reflectivity. Comparison of the intensity expected from simple reflection by the mirror (calculated from what is known about the mirror) with the intensity of radiation which also makes two traverses of the atmosphere (directly observed from satellite) should reveal the atmospheric transmission and thus many properties of the atmospheric constituents.

In this report we will show that it is theoretically feasible to make use of the sun glint to determine two important factors in atmospheric transmission: 1) the wavelength dependence of the aerosol extinction coefficient, and 2) the fractional selective absorption due to molecular constituents. We find that these two factors can be determined without ground-based calibration of the sun glint and in the presence of significant background effects. The techniques which can accomplish this are detailed in this report.

The analysis on which our results are based considers, in order, the properties of the mirror, the sources and magnitudes of background signals, the way in which atmospheric transmission combines with other factors to

determine the observed spectral radiances, and experimental measurements of spectral radiances which are needed to determine atmospheric transmission.

Properties of the Mirror (The Cox and Munk Model of the Sun Glint)

A perfectly flat sea surface would reflect an image of the sun with a radiance of approximately 2% that of the sun's disc (for near-normal to near-45° view angles). This reflected sunlight would constitute a small (10 milliradians in diameter) and extremely bright source (over 10^4 times as bright as the brightest cloud). However, the roughness of the sea surface degrades this image to a diffuse spot of much larger angular extent and much reduced radiance. A quantitative description of this effect is contained in the Cox and Munk model of the sun glint.[21]

According to Cox and Munk, the ratio of the sea surface radiance to the incident flux density is proportional to the probability of finding parts of the sea surface tilted so as to reflect sunlight to the observer, namely

$$R \equiv N/F = \frac{1}{4}\rho(\omega)\frac{\sec^4\beta}{\cos\mu}\, p(Z_x, Z_y) \qquad (3)$$

where the following notation is employed (see Figure 14):

R = sun glint scattering coefficient (sterad^{-1})

N = sea surface radiance (W - m^{-2} - μ^{-1} - sterad^{-1})

F = solar flux density (W - m^{-2} - μ^{-1})

ω = angle of incidence and reflection

β = sea surface tilt angle relative to local normal

Z_x, Z_y = components of local sea surface slope ($Z_x^2 + Z_y^2 = \tan^2\beta$)

μ = angle between observing direction and local vertical

$\rho_\lambda(\omega)$ = Fresnel reflection coefficient of sea water at angle ω and wavelength λ

$p(Z_x, Z_y)dZ_x dZ_y$ = probability of finding sea surface slopes with x and y components in the range $(Z_x, Z_x + dZ_x)$ and $(Z_y, Z_y + dZ_y)$.

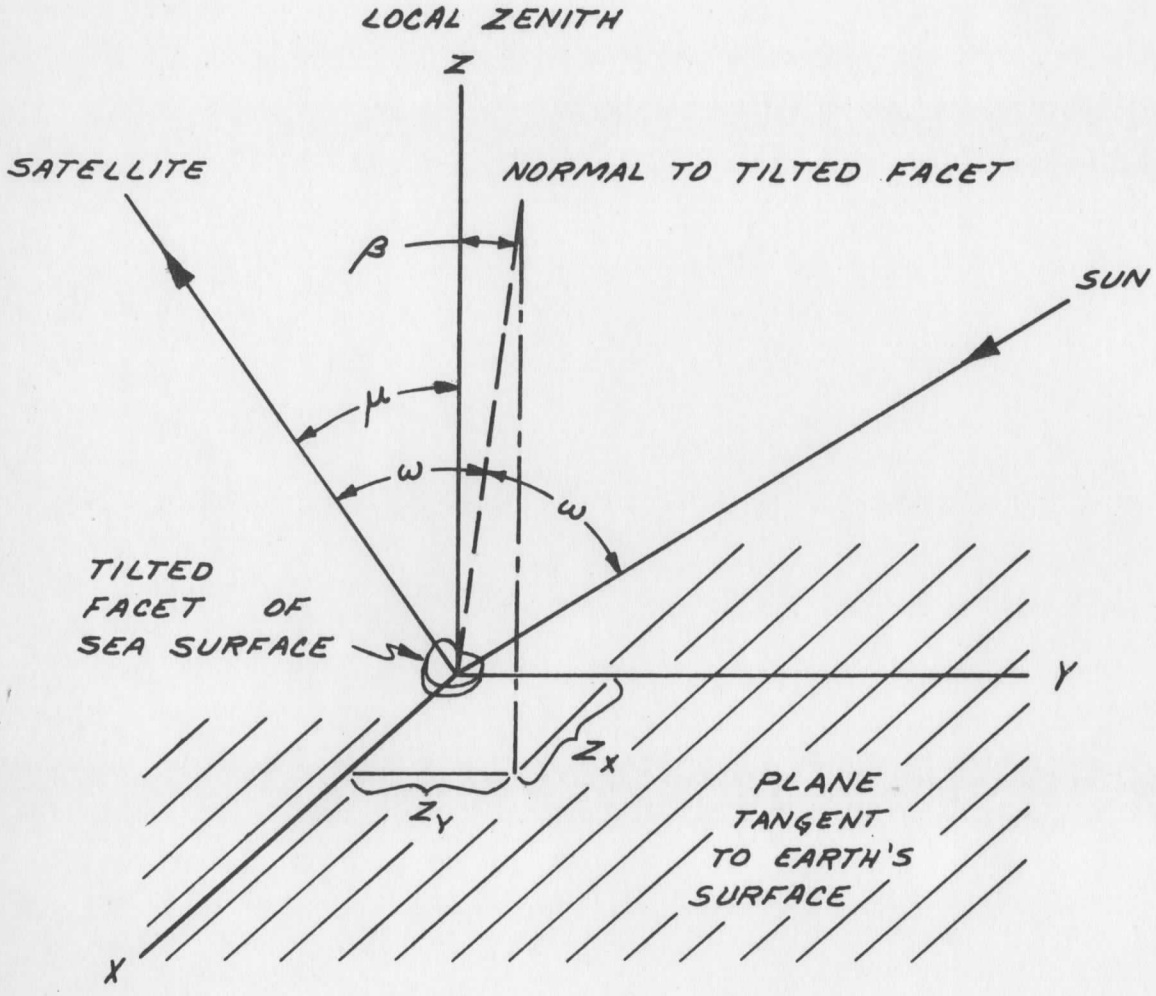

Figure 14. Geometry for calculating R, the sun glint scattering coefficient.

If the x and y axes are chosen to be aligned with the upwind and crosswind directions (denoted by u and c, respectively), the probability density takes the simple first-order form

$$p = (2\pi\sigma_c\sigma_u)^{-1} \exp(-\frac{1}{2}(Z_c^2/\sigma_c^2 + Z_u^2/\sigma_u^2)), \tag{4}$$

which is a two-dimensional gaussian function. Cox and Munk obtained the following empirical equations relating the widths to the surface wind speed:

$$\begin{aligned} \sigma_c^2 &= .003 + 1.92\times 10^{-3} W \pm .002 \\ \sigma_u^2 &= .000 + 3.16 \times 10^{-3} W \pm .004 \\ \sigma_c^2 + \sigma_u^2 &= .003 + 5.12 \times 10^{-3} W \pm .004 \end{aligned} \tag{5}$$

Here W is the wind speed in m/sec. This fit was made for wind speeds covering the range between 1 m/sec and 14 m/sec. Using this model, Levanon was able to estimate wind speeds using ATS-I data.[22] Recently Kornfield has been successful in using the asymmetry in (4) to determine wind direction as well.[23]

Since the crosswind asymmetry will not be significant to our subsequent discussions, we shall employ a somewhat simpler model for the probability density,

$$p = (\pi\sigma)^{-1} \exp(-1/\sigma^2 \tan^2\beta), \tag{6}$$

which results when σ_u and σ_c are assumed equal. The width in this one-dimensional model is just

$$\sigma^2 = \sigma_c^2 + \sigma_u^2 = .003 + 5.12 \times 10^{-3} W . \tag{7}$$

Substituting this latter result in Eq. (3) yields

$$R = \frac{1}{4} \rho_\lambda(\omega) \frac{\sec^4\beta}{\cos\mu} \frac{1}{\pi\sigma} \exp(-\tan^2\sigma/\sigma^2). \tag{8}$$

This model describes the broadening of the glitter pattern with increasing wind speed, and also the accompanying reduction in the peak of the sea surface radiance. Note that the maximum sun glint signal occurs for $\tan\beta = 0$ (the point of specular reflection for a calm sea), and has the form

$$R_{SP} = \frac{1}{4\pi\sigma} \rho_\lambda(\omega)\sec\mu , \tag{9}$$

where R_{SP} denotes the sun glint scattering coefficient at the specular point. The wind dependence of R_{SP} for $\mu = \omega = 0$ is shown in Figure 15. It is significant that the only wavelength dependence of R comes about through the Fresnel reflection coefficient $\rho_\lambda(\omega)$. Given the dependence of $\rho_\lambda(\omega)$ on λ we could thus determine the value of R at any wavelength by measuring it at only one. However there seems to be a significant disagreement between experimental results for $\rho_\lambda(\omega)$ even for pure H_2O, especially in the infrared region (Figure 16). There has been some recent work on the differential behavior of pure H_2O and sea water,[24] but this is of little use in absolute terms. In addition there is little information available on the variability of sea water over the globe or as a function of time. The frequency of surface slicks is particularly important information in this context.

Background Radiation

In addition to simple atmospheric attenuation, there are a number of extraneous background sources which can also modify the apparent brightness of the sun glint. These may be classified as follows:

1) skylight (molecular and aerosol), radiance = S_1F

2) sky glint (reflection of skylight by the sea surface), radiance = S_2F

3) sea light (solar radiance scattered by molecules and particulate matter in the sea), radiance = S_3F

4) foam light (solar radiation scattered by whitecaps), radiance = S_4F

5) black body radiation of the earth, radiance = B .

These sources are pictorially presented in Figure 17. Note that the first four are proportional to the extraterrestrial solar flux F as is the sun glint. Thus a comparison of these sources with the sun glint is readily made as a comparison of their effective scattering coefficients S_i with the sun glint scattering coefficient R .

1. Skylight

Extensive tables of the effective scattering coefficient for a plane parallel Rayleigh atmosphere have been compiled by Coulson, Dave and Sekera.[25] Their results include the effects of polarization and multiple scattering. However, except for optical depths greater than unity, little error is made by using a single scattering model (see Figure 18), which

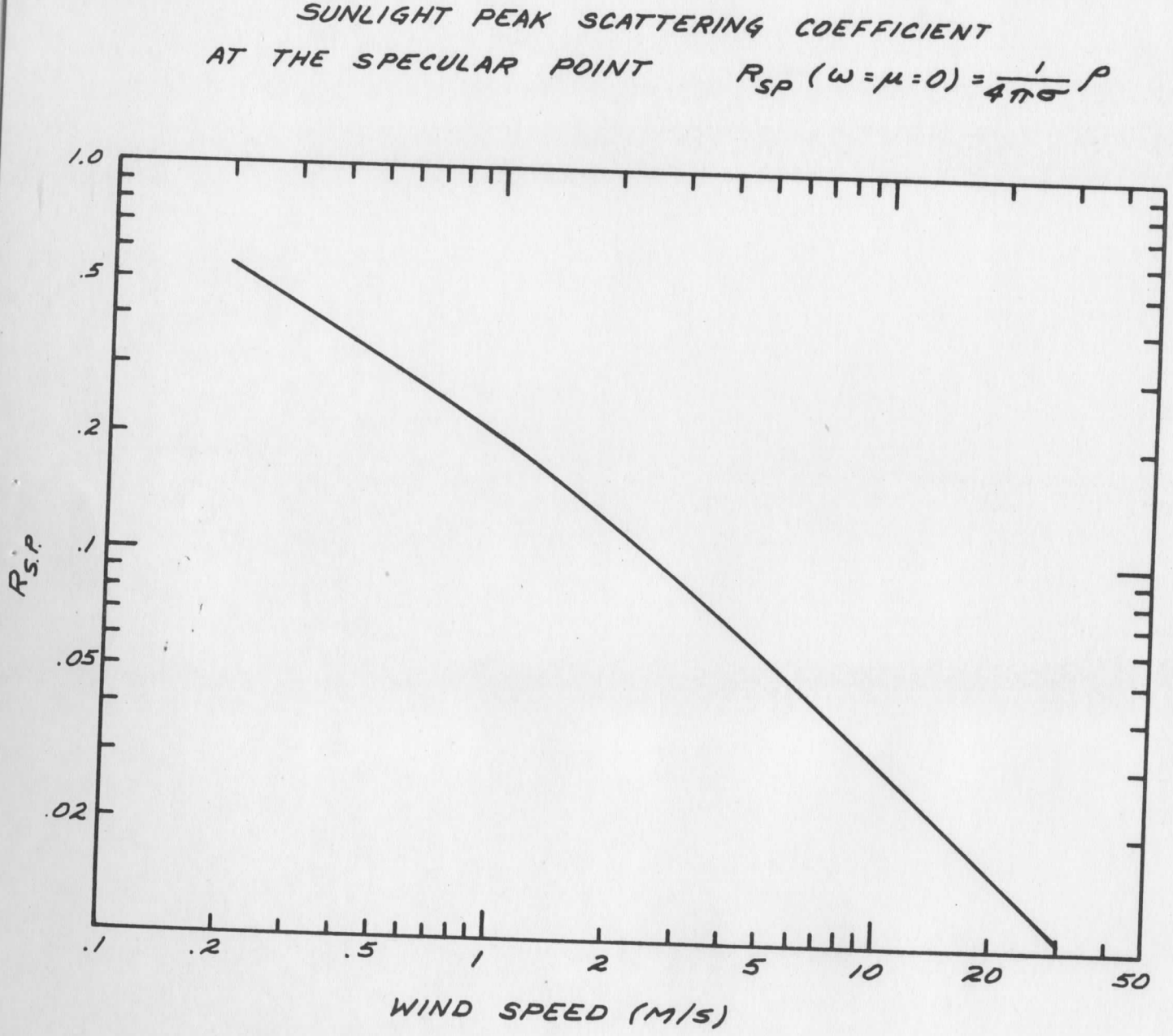

Figure 15. Dependence of the sun glint peak scattering coefficient on wind speed.

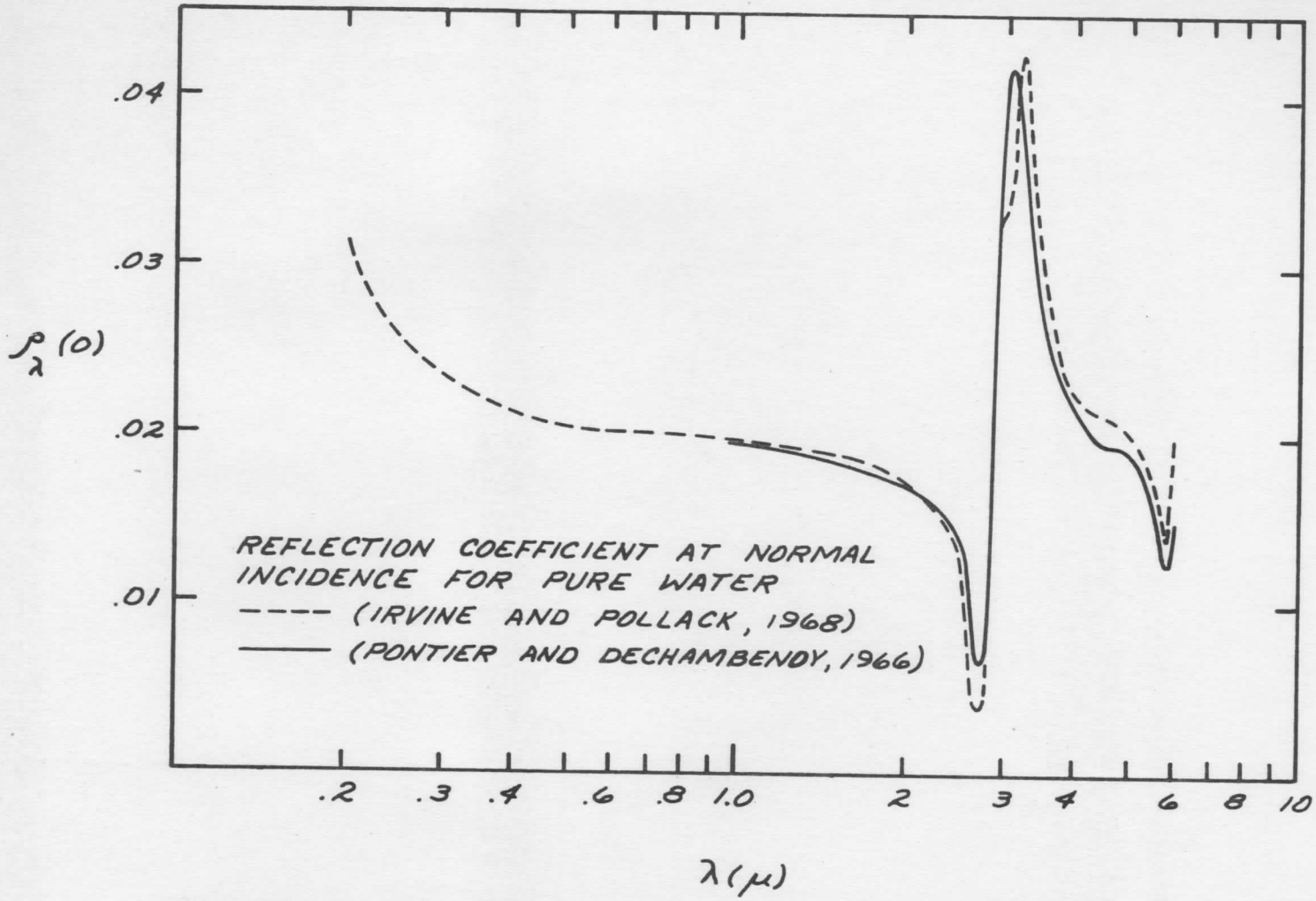

Figure 16. Wavelength dependence of $\rho_\lambda(\omega = 0°)$ for pure water.

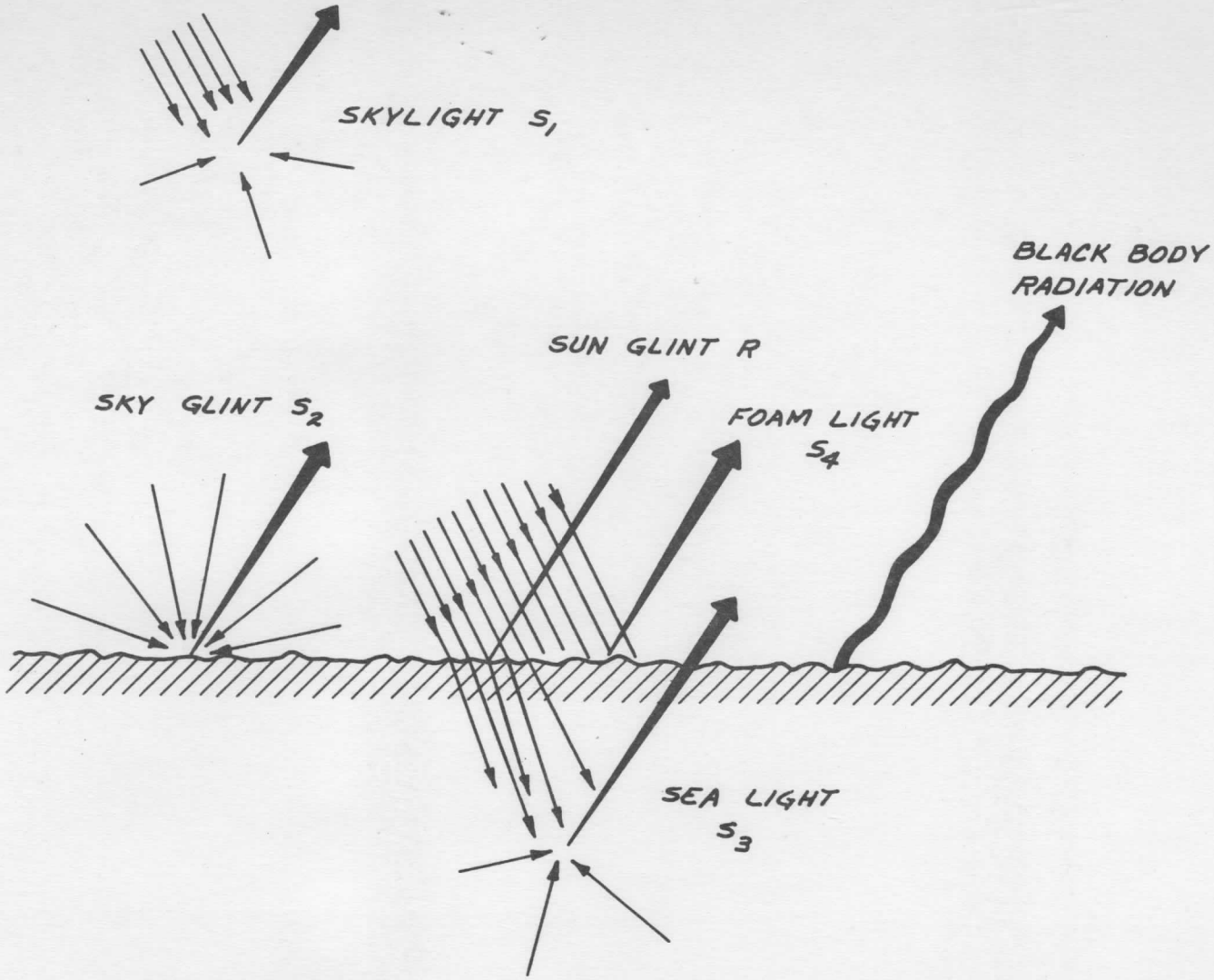

Figure 17. Sources of Background.

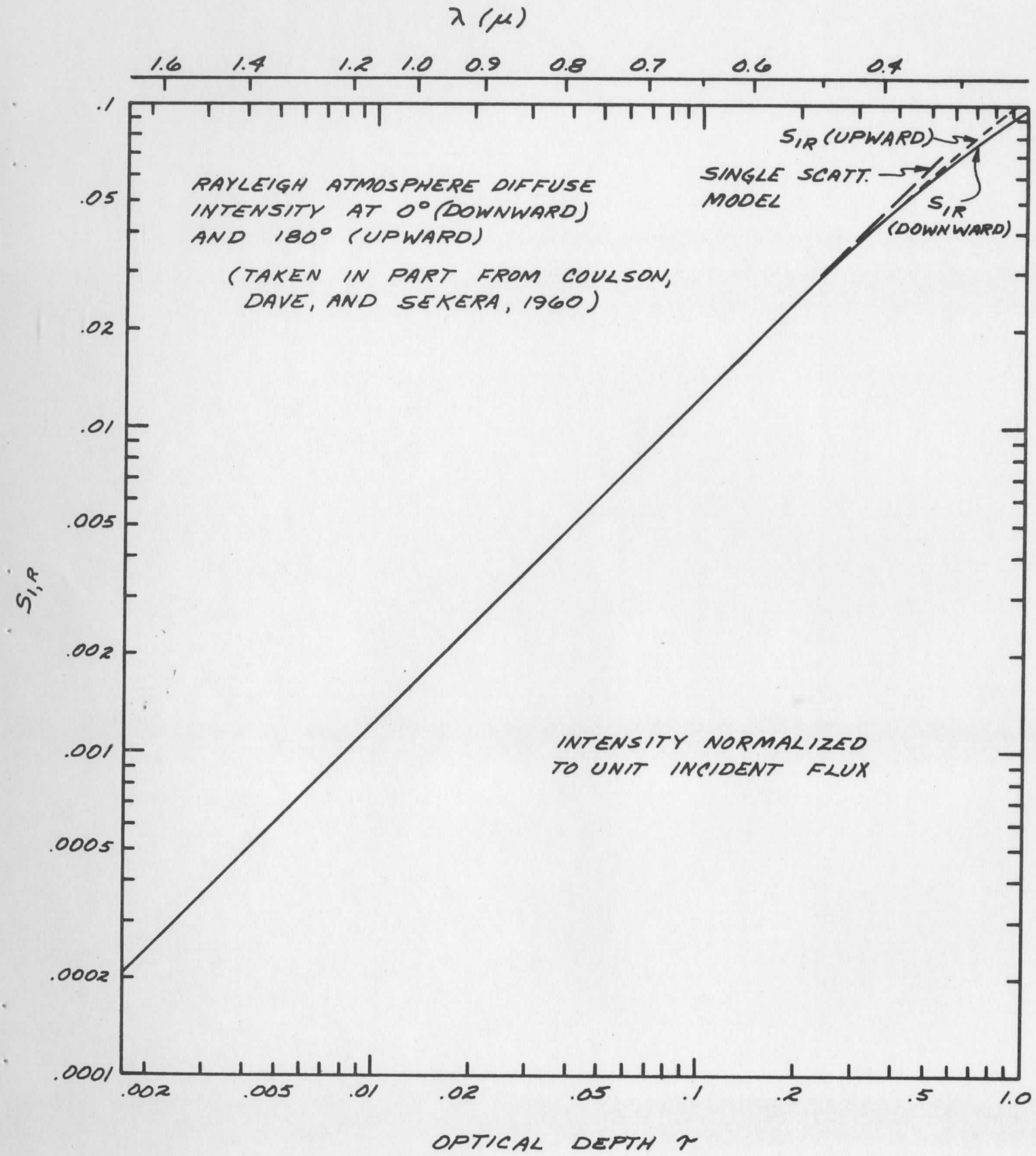

Figure 18. Rayleigh Scattering (exact and single scattering model)

has the advantage of great simplicity and easy inclusion of the aerosol component. For the purposes of a feasibility study, it is more than adequate. According to this model

$$S_1 = S_{1R} + S_{1A} = [\tau_{\lambda R} \frac{P_R(\theta)}{4\pi} + \tau_{\lambda A} \frac{P_A(\theta)}{4\pi}]M, \qquad (10)$$

where the subscripts R and A refer to the Rayleigh and aerosol components respectively, and

τ_λ = the attenuation coefficient (optical depth per unit air mass) at wavelength λ

$P_\lambda(\theta)$ = the scattering phase function at wavelength λ and scattering angle θ. (This is defined so that $\int P(\theta)d\Omega = 4\pi$.)

M = number of air masses in the line of sight.

The important and well-known facts of Rayleigh scattering may be summarized as

$$\tau_{\lambda R} \propto 1/\lambda^4$$

$$P_{\lambda R}(\theta) = 3/4\ (1 + \cos^2\theta)\ . \qquad (11)$$

The corresponding parameters of aerosol scattering are not so well known. Part of the problem results from the variability of both the number and size distribution of aerosol particles. We shall conduct this feasibility study on the basis of what might be considered as typical aerosol properties for maritime environment, although there is considerable uncertainty in deciding what is typical. The attenuation measurements of Volz,[26] and Quenzel[27] lead us to believe that we will not be too far wrong to assume that $\tau_{A,\lambda} = 0.1$ for $\lambda = .7\mu$, and that the wavelength dependence of τ_λ (which appears to be fairly flat in the visible region) and of $P_{\lambda A}(\theta)$ are approximately described by Deirmendjian's haze model M.[19] In general, $P_A(\theta)$ is two orders of magnitude larger than $P_R(\theta)$ in the forward direction, and an order of magnitude smaller in the backward direction (Figure 8). This makes aerosols easy to see from the surface (as in the sun's aureole) and difficult to see from a satellite. At increasing wavelengths, aerosol scattering falls off much more slowly than Rayleigh scattering and eventually becomes the dominant component of skylight, regardless of the angle of observation.

2. Sea Light

The radiant intensity of light leaving the interior (or the effective scattering coefficient S_3) depends not only on the scattering in the interior but also on the character and depth of the underlying surface. Cox and Munk made an estimation of this term from their measurements, but their failure to account for scattering in the atmosphere between their plane at 2,000 feet and the surface makes interpretation of their results difficult. However, a rough estimate of this term can be obtained from the Monte Carlo calculations of Kattawar and Plass[28] which show that

$$S_3(\lambda = .46\mu) \approx .01$$

$$S_3(\lambda = .65\mu) \approx .001 . \qquad (12)$$

This variation with wavelength is consistent with the order of magnitude increase of the absorption coefficient from its minimum at $\lambda = .46\mu$ to its value at $\lambda = .65\mu$. A crude model of this behavior can be made when the scattering cross-section is much less than the absorption cross-section. Under these conditions we have

$$S_3(\lambda, \theta) \approx \int_0^{Z_{max}} \frac{d\sigma_{scatt}(\theta)}{d\Omega} e^{-2\beta_{ext} Z} n(Z)dZ \propto \frac{1}{\beta_{ext}} \frac{d\sigma_{scatt}(\theta)}{d\Omega} \qquad (13)$$

where $d\sigma/d\Omega$ is the scattering cross section, $n(Z)$ is the number of scatterers per unit volume at depth Z, β_{ext} is the extinction coefficient of sea water, and Z_{max} is the ocean depth. Since β_{ext} rapidly increases six or seven orders of magnitude into the infrared (Figure 19), we are led to expect a correspondingly rapid decrease in S_3.

3. Sky Glint

According to Cox and Munk, the radiance of the sea surface due to reflected skylight (N') is given by

$$N' = \sec\mu \iint N_s \rho(\omega) \cos\omega \sec\beta \, p(Z_x, Z_y) dZ_x dZ_y , \qquad (14)$$

where N_s is the radiance of the sky in the direction determined by Z_x and Z_y. The limits of integration are set to include all visible slopes. For near nadir observation ($\sec\mu \approx 1$) and using Eq. (6) for $P(Z_x, Z_y)$, the integrand in Eq. (14) becomes azimuthally symmetric about the zenith. Under these conditions, Eq. (14) reduces to

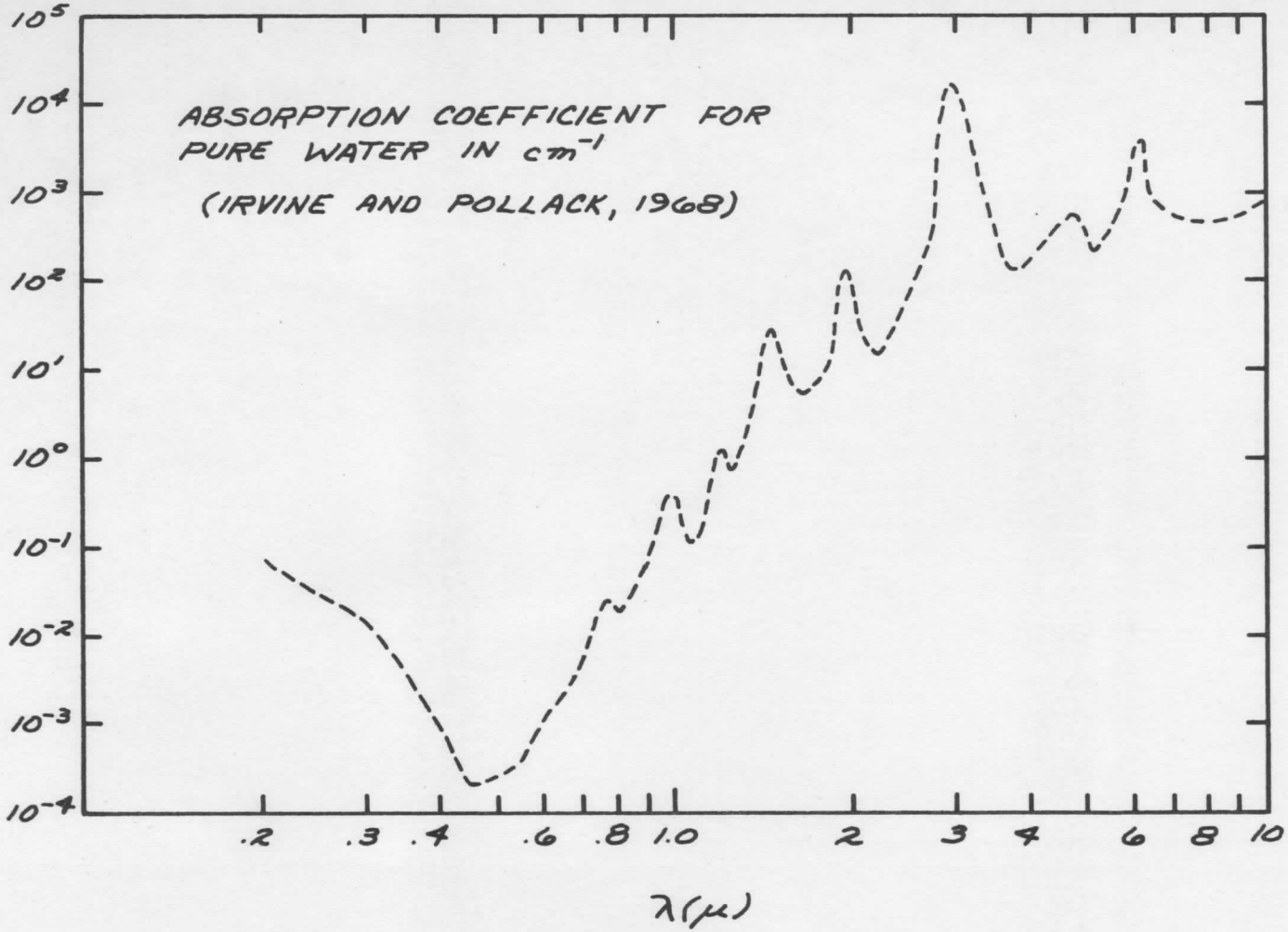

Figure 19. Wavelength dependence of the extinction coefficient for pure liquid water.

$$N' = \int_0^{\eta_{max}} \eta d\eta \frac{2}{\sigma^2} e^{-\eta^2/\sigma^2} \rho(\beta) N_s(\beta) \tag{15}$$

where $\eta = \tan\beta$. The quantity η_{max} is usually somewhat less than $\tan \pi/4 = 1$. However, even for reasonably large winds, taking $\eta_{max} = \infty$ will not significantly affect Eq. (15) because of the exponential cutoff for large η^2/σ^2. Obviously the sea surface brightness depends not only on the sky radiance but also on its distribution as a function of zenith angle (which has the same value as β in this case). (Since $\rho(\beta)$ is a very weak function of β except near $\beta = 90°$, its angular dependence plays no role for a vertical viewing geometry.)

For a sky of uniform radiance, N_0, Eq. (15) may be integrated exactly to yield

$$N' = N_0 \rho(0°) \tag{16}$$

an eminently reasonable wind independent result.

For a Rayleigh sky the results are very similar:

$$N' = \rho(0°) N_s(0°)[1 + 2.8\sigma^4 + \ldots] \approx \rho(0°) \frac{\tau_R}{4\pi} P_R(0°) F \tag{17}$$

This shows a small but negligible dependence on wind.

For an aerosol sky the results are quite different. If τ_A and $P_A(\theta)$ are the aerosol optical depth per unit air mass and phase function, respectively, then the aerosol component of the sky glint is given by

$$N' = \frac{2\tau_A \rho}{2\pi\sigma^2} \int_0^{\eta_{max}} \eta d\eta \left[e^{-\eta^2} \frac{P_A(\beta)}{4\pi} \sec\beta\right] F, \tag{18}$$

where $\rho = \rho(0°) \approx \rho(\beta)$ for $\beta \lesssim 30°$.

Using Diermendjian's haze model M for $P_A(\theta)$ at $\lambda = .7\mu$, we find the results expressed in the following table:

W(m/s)	σ	$\sigma N'/2\rho\tau_A F$
.006	.0577	.089
1.40	.100	.103
5.40	.173	.103
11.40	.245	.096

The mean behavior is described by the relation

$$N' \approx \frac{2\rho\tau_A}{\sigma} C_\lambda F, \qquad \text{haze model M,} \tag{19}$$

where $C_\lambda = .098$ at $\lambda = .7$. This relation does not hold at all wavelengths because $P_A(\theta)$ varies as well as τ_A . (Figure 17.)

In terms of scattering coefficients we may summarize these results as

$$S_2 = S_{2R} + S_{2A} \quad \text{where}$$

$$S_{2R} \approx \rho(\omega) \frac{\tau_R}{4\pi} P_R(\mu) \tag{20}$$

$$S_{2A} \approx 2\rho(0°) \frac{\tau_A}{\sigma} [.098], \quad \lambda = .7\mu . \tag{21}$$

Note that we have included here an approximate form for the angular dependence of S_{2R} , which we have not proven.

4. Foam Light

Using data reported by Woods Hole Oceanographic Institute and by the Visibility Laboratory of the Scripps Institute of Oceanography, Duntley has made an empirical fit for the fractional area of the sea surface covered by white water as a function of wind speed.[29] This is shown in Figure 20. To determine the surface radiance due to foam light we must also know the scattering properties of foam (or white water), which may depend upon the wind speed and perhaps other parameters as well. For lack of better information we shall assume that foam is a wavelength independent lambertian reflector with albedo one, which is very probably an overestimate of the scattering power of this source. Under these assumptions we have

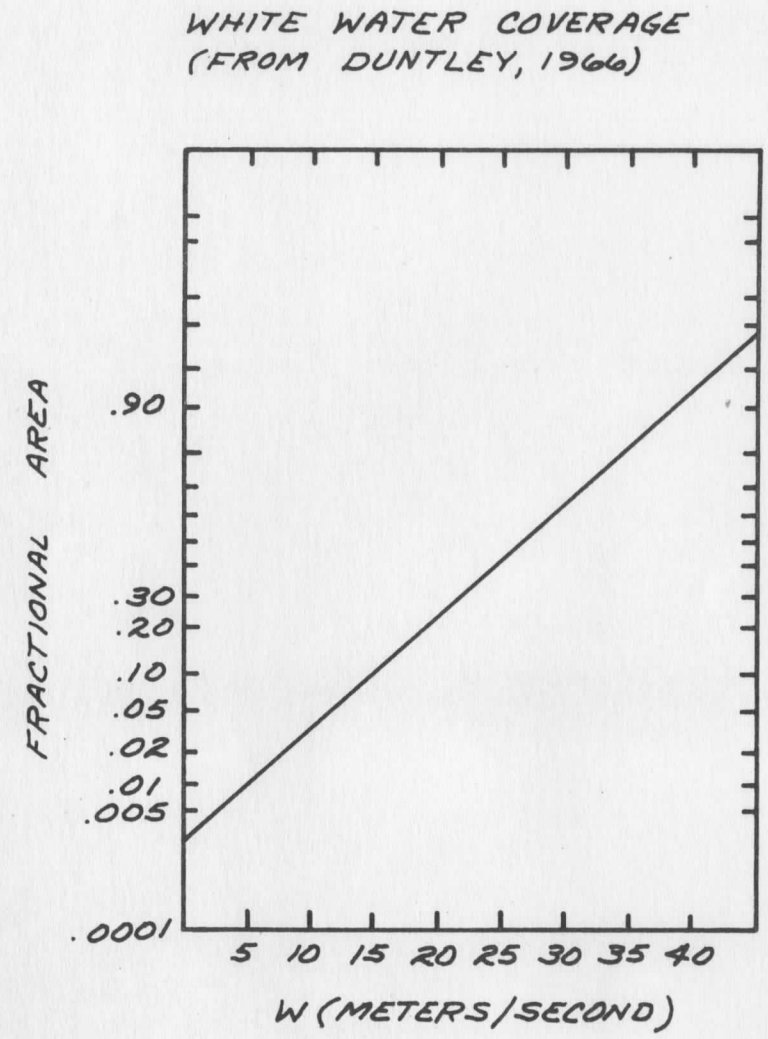

Figure 20. Fractional horizontal area of sea surface covered by white water (foam).

$$S_4 = \frac{f}{\pi} \cos \theta_s \qquad (22)$$

where θ_s = sun zenith angle and f is the fraction of horizontal area covered by foam. It should be noted that S_4 increases rapidly with increasing wind speed, while the sun glint scattering coefficient decreases with increasing wind speed. For high enough winds this source will thus become larger than the sun glint signal.

5. Black Body Radiation

In the absence of incident irradiance, the spectral radiance of a surface of emissivity ϵ_s at absolute temperature T is given by

$$N_B = \epsilon_s B(\lambda, T) = \epsilon_s \frac{c_1}{\lambda^5} [e^{c_2/\lambda T} - 1]^{-1}, \qquad (23)$$

where $c_1 = 1.1909 \times 10^{-12}$ W cm^2 sterad^{-1} and $c_2 = 1.4380$ cm° K. The sea surface may be taken to have an emissivity of one, except when white water is significant. The black body radiation of the sea surface, which peaks near $\lambda = 10\mu$ is comparable to reflected solar radiation in the vicinity of $\lambda = 4\mu$. For much longer wavelengths this source is dominant, and for much smaller wavelengths it is negligible. This fact affords us the possibility of calibrating the sun glint by comparing it to the earth's black body radiance, provided the latter can be well determined from satellite (perhaps by measurements in the 10μ region). For a presentation of the concepts involved in such an experiment, see Reference 1.

Summary of Background

A useful summary of the relative sizes of the background sources and the sun glint is presented in Figure 21, which shows the wavelength dependence of all scattering coefficients for typical observing conditions. These conditions are taken to be: a surface temperature of 300° K, a wind speed of 5 m/s, and a vertical viewing geometry (the sun and satellite at the zenith of the observed point). In this figure it is the scattering coefficient at the center of the sun glint pattern which is plotted.

For the most part, skylight is the major source of background radiance. Beyond $\lambda = .7\mu$ sea light and Rayleigh sky glint are completely negligible. Beyond 4μ black body radiation becomes dominant. Atmospheric transmission factors have been included to show the relative background strengths as

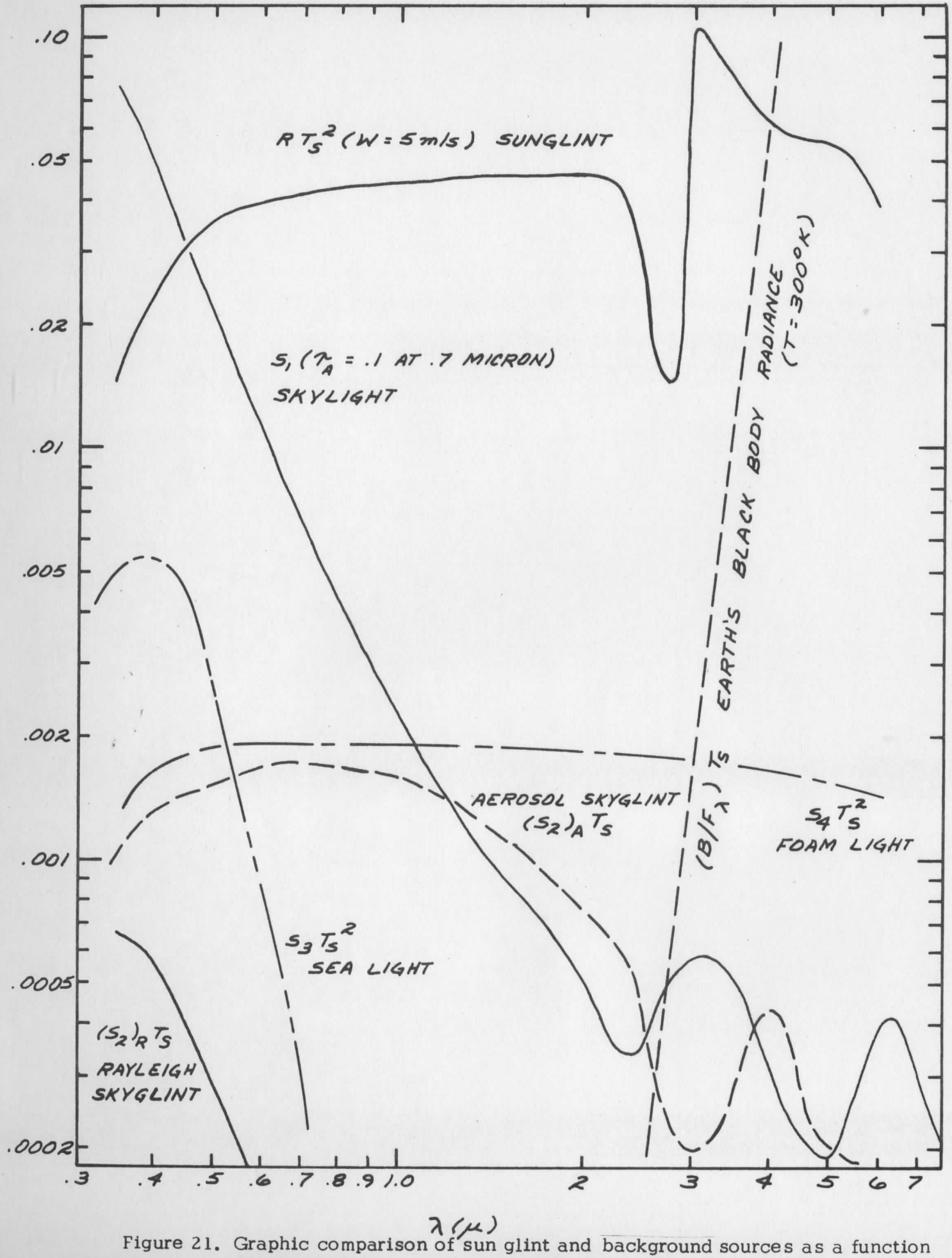

Figure 21. Graphic comparison of sun glint and background sources as a function of wavelength.

viewed from a satellite. The description of these factors and how they influence sun glint measurements is dealt with in the following section.

The Generalized Sun Glint Experiment

As we have already seen, any measurement of the sun glint radiance contains radiance contributions from other sources. If one could make one measurement with the sun glint on and one with all conditions the same except that the sun glint is "turned off," the background could be removed by subtraction. A crude approximation to this method is to make one measurement at the peak of the sun glint and one where (or when) the sun glint is negligible. This implies two measurements for every sun glint determination.

If one is interested in the wavelength dependence of atmospheric transmission, at least two more measurements are required—one at a reference wavelength λ, and one at the wavelength of interest λ'. This is necessary to reduce further the effects of background, or to "calibrate" the sun glint. Thus there are generally four measurements in a sun glint experiment: for each of two wavelengths, two measurements with different viewing geometries.

The two measurements with different geometries can be made in basically three different ways, each with its own deficiencies. These are:

a) Sun fixed, satellite fixed; measurements made at two different view angles (and thus at two different points on the surface).

b) Sun fixed, satellite moves; measurements made at two different view angles of the same point on the surface (and at two different times).

c) Satellite fixed, sun moves; measurements made at same view angles of same surface point at two different sun angles (and at two different times).

A diagrammatic presentation of these cases is made in Figure 22. Method a), which corresponds to taking a snapshot of the sun glint pattern, has the disadvantage of looking at two different points on the surface which, at satellite altitude, must be so far apart that local conditions (wind speed, for example) are very likely to be significantly different. In addition, background corrections are more difficult because two different air masses are in view (at different angles as well).

Methods b) and c) both have the advantage of viewing the same surface point. However, in b) different air masses are viewed, and in c) the incident flux travels through different air masses. In addition, c), which is

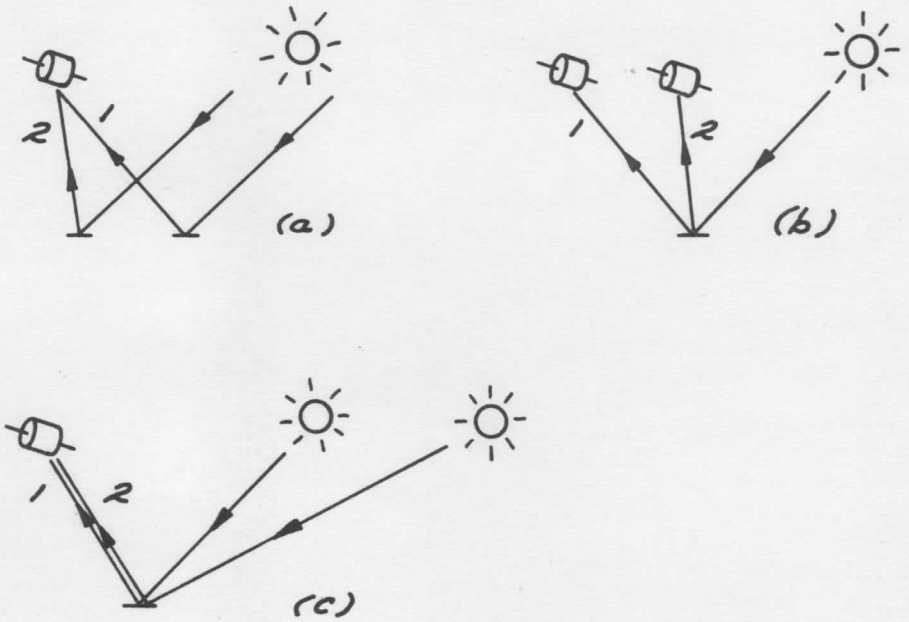

Figure 22. Sun Glint Experimental Geometries

only possible for a geosynchronous platform, requires that measurements be separated in time by several hours, although Levanon's and Kornfield's work indicates that local variations in this time span are not generally significant.

Transmission Factors

The discussion of atmospheric attenuation, and the corresponding transmission factors, has been delayed until this point because it affects each source in a different way. We shall deal with two fundamentally different transmission factors:

1) T_s describes the attenuation due to scattering (from molecules and aerosols).

2) T_a describes the attenuation due to molecular band absorption. Since these are independent processes in the single scattering approximation, the net one-way transmission of the atmosphere is $T_s T_a$. For two-way transmission we shall use the notation T_{2s} and T_{2a}, in which case the net two-way transmission is $T_{2s} T_{2a}$. When the incoming and outgoing paths are identical (vertical viewing geometry, for example), $T_{2s} = T_s^2$; but $T_{2a} \neq T_a^2$ except for bands of weak nonoverlapping lines. The wavelength dependence of the scattering transmission factors is shown in Figure 23 for a colinear vertical viewing geometry.

Additional notation is needed to describe the effects of molecular absorption on directly scattered light (i.e., skylight). For this we shall add the subscript s so that the appropriate transmission factors are T_{as} for skylight seen from above, and T_{2as} for skylight reflected by the sea surface. The actual effective optical paths in these cases depends upon the relative optical thicknesses of the Rayleigh and Mie scatterers and their distributions in altitude.

We are now in a position to write down the expressions for the four radiances measured in a general satellite sun glint experiment. These are

$$N_1 = [T_{as} S_1 + T_s T_{2as} S_2 + T_{2s} T_{2a} (S_3 + S_4 + R)]F + T_s T_a B \tag{24}$$

$$N'_1 = [T'_{as} S'_1 + T'_s T'_{2as} S'_2 + T'_{2s} T'_{2a} (S'_3 + S'_4 + R')]F' + T'_s T'_a B' \tag{25}$$

$$N_2 = [T^{(2)}_{as} S^{(2)}_1 + T^{(2)}_s T^{(2)}_{2as} S^{(2)}_2 + T^{(2)}_{2s} T^{(2)}_{2a} (S^{(2)}_3 + S^{(2)}_4 + R^{(2)})]F$$

$$+ T^{(2)}_s T^{(2)}_a B^{(2)} \tag{26}$$

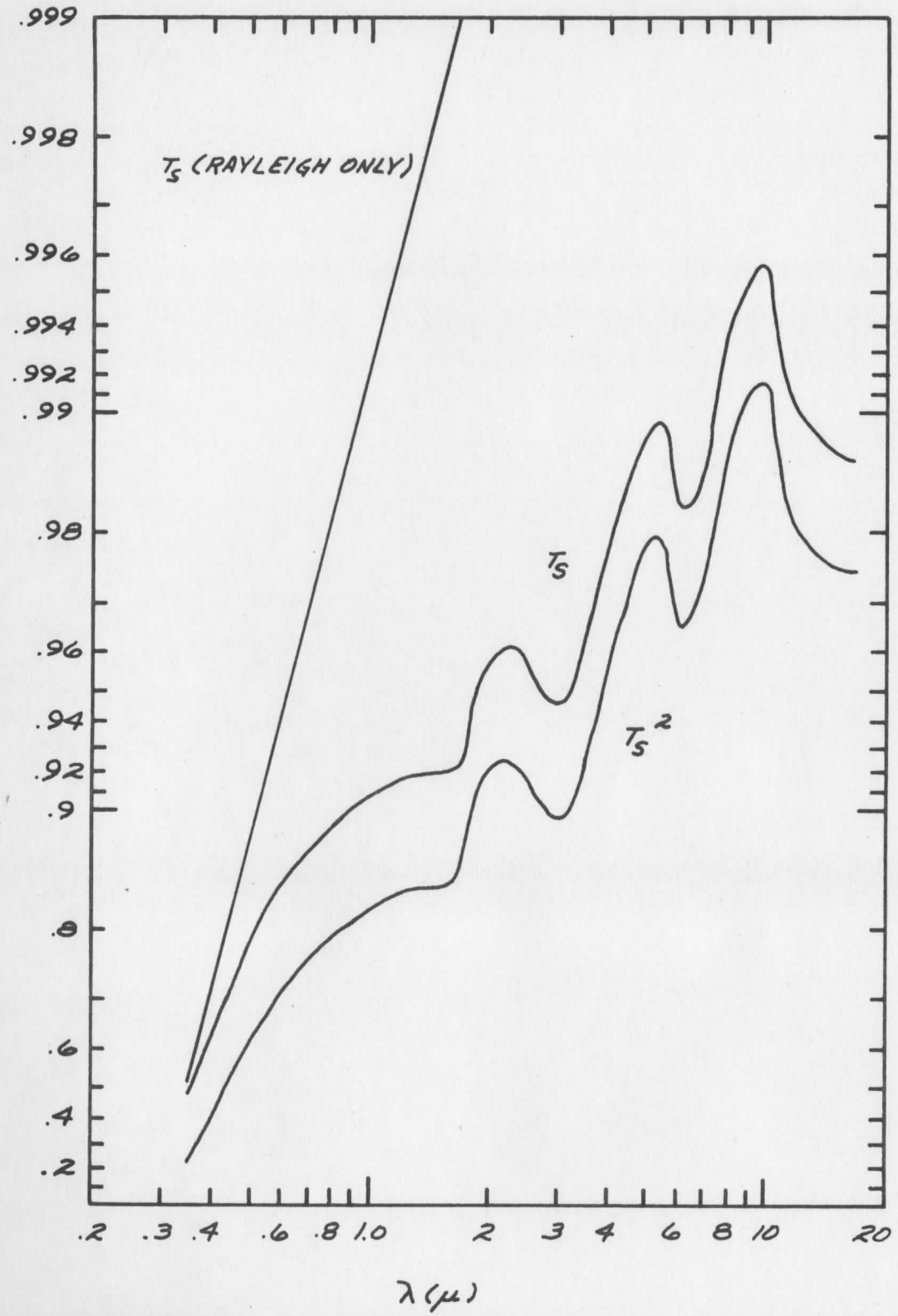

ATMOSPHERIC TRANSMISSION DUE TO MOLECULAR (RAYLEIGH) AND AEROSOL (MIE) SCATTERING, FOR HAZE MODEL M NORMALIZED TO $\tau_A = 0.1$ AT 0.5 MICRON.

Figure 23. Scattering Transmission Factors

$$N'_2 = [{}^{(2)'}_{as}S_1^{(2)'} + T_s^{(2)'}T_{2as}^{(2)'}S_2^{(2)'} + T_{2s}^{(2)'}T_{2a}^{(2)'}(S_3^{(2)'} + S_4^{(2)'} + R^{(2)'})]F'$$

$$+ T_s^{(2)'}T_a^{(2)'}B^{(2)'} \qquad (27)$$

where the unprimed measurements are at wavelength λ and the primed at wavelength λ'. Given F and F' we have four equations in fifty-four unknowns. It is obvious that we cannot determine all these factors from satellite-based measurements. However, since the backgrounds are generally small compared to the sun glint, even a relatively crude model for their angular and wavelength dependence can be used to reduce the number of unknowns to a manageable level. The details will be discussed for four separate experiments designed to measure distinctly different parameters.

Determination of R

As an example of techniques which can be used in the visible and near-infrared spectral regions, we shall consider the problem of measuring wind speed from geosynchronous altitude using method c). Actually R is measured and from this the wind speed is determined from Eq. (3) and (5).

Avoiding regions of ozone absorption and molecular band absorption, we may assume $T_a = 1$ and $B = 0$ for $.4\mu \leq \lambda \leq 2.5\mu$. The spectral radiance measurements at two different sun angles are then

$$N_1 = [S_1 + T_2S_2 + T_{2s}(S_3 + S_4 + R)]F \qquad (28)$$

$$N_2 = [S^{(2)} + T_2^{(2)}S_2^{(2)} + T_{2s}^{(2)}(S_3^{(2)} + S_4^{(2)} + R^{(2)})]F\,. \qquad (29)$$

Let us assume that the second measurement is made at a sun angle sufficiently large so that $R^{(2)} = 0$, and also that the satellite is at the zenith of the observed point. We may also assume that $S_{2A}^{(2)} = 0$. (Because of the highly peaked forward scattering of aerosols, if the sun's image is out of view, the aureole's image will be also.) Under these conditions, Eq. (28) and Eq. (29) become

$$N_1 = [S_1 + T_sS_{2R} + T_s^2(S_3 + S_4)]F + [T_sS_{2A} + T_s^2R]F \qquad (30)$$

$$N_2 = [S_1^{(2)} + T_sS_{2R}^{(2)} + T_sT_s^{(2)}(S_3^{(2)} + S_4^{(2)})]F\,. \qquad (31)$$

For reasonably small sun angles $S_1^{(2)}$, $S_{2R}^{(2)}$, $S_3^{(2)}$, $S_4^{(2)}$ are all approximately linear in the cosine of the sun zenith angle. Furthermore, if the optical depth per unit air mass τ is not close to unity $T_s^{(2)}$ will not be much different from T_s. Thus it is reasonable to suppose that we can find a geometrical function $f(1,2)$ which relates the backgrounds at two different sun angles, i.e.

$$[S_1^{(2)} + T_s S_{2R}^{(2)} + T_s T_s^{(2)}(S_3^{(2)} + S_4^{(2)})] \approx f(1,2)[S_1 + T_s S_{2R} + T_s^2(S_3 + S_4)] \tag{32}$$

(In the case we are discussing, $f(1,2) \approx \cos(\theta_s)$, where θ_s is the solar zenith angle at the observed point.) Using Eq. (32) it becomes possible to subtract out most of the background terms, i.e.

$$\frac{1}{F}\left[N_1 - \frac{1}{f(1,2)} N_2\right] = T_s S_{2A} + T_s^2 R \tag{33}$$

Since both the sun glint and aerosol sky glint peak at the specular point and fall off rapidly away from this, we have been unable to separate these two components, as shown in Eq. (33). In principle, a detailed study of the angular distribution of the left-hand side of Eq. (33) away from the specular point should make this distinction possible. However, there are some practical difficulties in doing this. Since S_{2A} is relatively small compared to R, the difference between the angular distribution of $T_s^2 R$ and that of $T_s S_{2A} + T_s^2 R$ may very well be negligible, especially in view of the difficulty in determining what the angular dependence of RT_s^2 ought to be.

In the Cox and Munk model (Eq. 3) knowing the peak value of R determines its angular distribution. However, we cannot directly measure the peak value because of the contamination of aerosol sky glint. Furthermore, since Cox and Munk observed at an altitude of 2,000 ft and made no explicit correction for aerosols, it is only reasonable to assume that their model itself contains the aerosol sky glint term for an unknown aerosol optical thickness τ_A. Thus, in using the Cox and Munk model to determine winds, it is probably more reasonable to use, instead of Eq. (33), the expression

$$T_s^2 R_{c.m.} = \frac{1}{F}\left[N_1 - \frac{1}{f(1,2)} N_2\right], \tag{34}$$

where

$$R_{c.m.} = \frac{1}{T_s} S_{2A} + R \quad . \tag{35}$$

Note that in principle R is independent of τ_A, while $R_{c.m.}$ depends on τ_A, and thus the two-dimensional gaussian model for $R_{c.m.}$ (which we previously used for R) cannot be expected to hold for τ_A significantly different from the aerosol optical thickness typical of the Cox and Munk measurements (which is not known). From our knowledge of τ_R and a reasonable estimate of τ_A we can estimate T_s^2 and thus $R_{c.m.}$ (and the wind speed). In principle this description applies to the methods used by Kornfield to correct for background. His results attest to the feasibility of the technique applied to ATS-I measurements.

Determination of Aerosol Extinction

We shall now consider a technique for using the sun glint to measure that component of Ts due to aerosols. Since the Rayleigh optical depth $\tau_{R,\lambda}$ can be calculated, a measurement of $Ts = \exp(-\tau_{R,\lambda})\exp(-\tau_{A,\lambda})$ determines $\tau_{A,\lambda}$, the aerosol optical depth (or extinction coefficient per unit air mass). Consider four measurements, two of the type just described at each of two wavelengths λ, λ'. After the background subtraction techniques (Eq. (33)) are employed, we have the two equations

$$T_s^2\left(\frac{1}{T_s} S_{2A} + R\right) = A \tag{36}$$

$$T'_{2a}T'^2_s\left(\frac{T'_{2as}}{T'_{2a}T'_s} S'_{2A} + R'\right) = A', \tag{37}$$

where A and A' are known from measurements at λ and λ'.

Since $R/R' = \rho_\lambda/\rho'_\lambda$ we may eliminate R and R' from this pair of equations to obtain

$$\frac{T'^2_s}{T_s^2} = \frac{\rho_\lambda}{\rho'_\lambda}\frac{A'}{A}\left[\frac{1 - T'_s\dfrac{S'_{2A}}{A'}}{1 - T_s\dfrac{S_2A}{A}}\right] \tag{38}$$

The contributions from aerosol skylight, S_{2A} and $S_{2A'}$, are typically of the order of a few percent of R (Figure 21). Thus we may neglect second order products of S_{2A}/A and S_{2A}/A' compared to one. Employing Eq. (19) also, we may write Eq. (38) as

$$e^{-x} \approx \alpha[1 - x\beta + O(10^{-3})], \tag{39}$$

where

$$x = 2(\tau_A - \tau'_A)$$

$$\alpha = \frac{\rho_\lambda A'}{\rho'_\lambda A} e^{-2(\tau_R - \tau'_R)}$$

$$\beta = \frac{1}{\sigma}\left[\frac{\rho_\lambda C_\lambda e^{-(\tau_R + \tau_A)}}{A}\right]_{\text{mean}} \tag{40}$$

The mean indicated is for the two wavelengths λ and λ'. The reflectivities ρ_λ and ρ'_λ can be obtained from Figure 16. The sea surface slope distribution width σ can be obtained approximately (probably better than 10% accuracy) from Eq. (36) or Eq. (37), even neglecting S_{2A}. The factor C_λ depends on the haze model used (or observed) as well as wavelength, but can probably be estimated to within 10-20%. Since τ_A is of the order of 0.1, the mean of $e^{-\tau A}$ can be estimated probably to within 10% or 20%. The Rayleigh optical depths are assumed to be well known.

Neglecting for the moment the possible measurement errors in A' and A the major source of error is due to uncertainties in β which may be of the order of 30% or more. Even if uncertainties are considerably larger than this, they may be reduced to this level or below through iteration of Eq. (39). The effect of this uncertainty in β on the determination of X may be obtained from Eq. (39) by differentiation.

$$\frac{dX}{X} = \frac{d\beta}{\beta}\left[\frac{1}{\frac{1}{\alpha\beta}e^{-X} - 1}\right] \tag{41}$$

Under the observing conditions for which Figure 21 applies $\alpha\beta \approx \beta \approx .04$ and $X \approx .1$. Thus we have

$$\frac{dX}{X} \approx \frac{d\beta}{\beta} \times .05, \tag{42}$$

which means that a 30% error in β results in a 1.5% error in X. This would correspond to changes in aerosol optical thickness as function of wavelength of about .002 out of .1. Even a factor of two error in β would lead to an error in $\tau_A - \tau'_A$ of only .005 (or 5%). Thus we see that any reasonable uncertainty in β will not lead to significant errors in the determination of $\tau_A - \tau'_A$. Errors resulting from imperfect background subtraction, spectral radiance measurement errors, and, in some cases, uncertainties in the ratio $\rho_\lambda/\rho'_\lambda$ will be most significant.

Returning to equations (30) through (33), we may estimate the effects of uncertainties in the background subtraction techniques. This effect is most important in the visible region of the spectrum since the background is largest there (Figure 22). For our standard observing conditions (those for which Figure 22 applies), the total background contribution other than aerosol skylight is roughly 25% of RT_s^2 at $\lambda = .6\mu$. At $\lambda' = 1.0\mu$ this amounts to only about 3%. If the function $f(1, 2)$ which relates the backgrounds at two different observing geometries (Eq. (32)) describe background variations only to within 10% of the total background (which is a considerable error), the effect would show up on the right-hand side of Eq. (33) as 2.5% radiance change at $\lambda = .6\mu$ and .3% change at $\lambda' = 1.0\mu$. For the two wavelengths chosen as examples here, this effect could be seen in Eq. (40) as a 3% (approximately) error in α. Taking differentials of X and α we find (ignoring β variations) that

$$dX \approx d\alpha \tag{43}$$

Since $\alpha \approx 1$, a 3% error in α corresponds to $d\alpha \approx .03$, and similarly the error in $X = \tau_A - \tau'_A$ is approximately .03 out of .1, or about 30%. This may seem like a large error, but this can still be useful in detecting large changes in aerosol concentration (which are quite frequent)[26]. It is also likely that errors in background subtraction will be considerably smaller than we have assumed here.

The effect of errors in the spectral radiance measurements are related to the error in X through Eq. (33), (36), (37), (38), (39), and finally (43). We have, neglecting the other errors present,

$$dX \approx d\alpha \approx 4\frac{dN}{N} \tag{44}$$

where dN/N is the average percentage r. m. s. error for the four radiances used in these computations. Thus a 1% error in radiance measurements produces an error in $X = \tau_A - \tau'_A$ of approximately .04 out of a probably variation of .1 (from λ to λ'). This indicates that instrumental requirements will be severe. We hope to deal with this aspect of the problem in a later report.

Thus we conclude that measurement of aerosol optical thickness changes with wavelength ($\tau_A - \tau'_A$) is theoretically feasible using the sun glint. For typical observing conditions (Figure 22), this change should be measurable to within .02 to .03 if adequate instrumentation is available (spectral radiance measurement error no greater than about .25%).

Determination of $\tau_{A,\lambda} - \tau_{A,\lambda'}$ does not, of course, determine the absolute values of either $\tau_{A,\lambda}$ or $\tau_{A,\lambda'}$. To determine this directly, an

absolute calibration of the sun glint would be required. Since this presents considerable difficulties, it is fortunate that there are indirect methods. First one can choose λ' large enough to insure that $\tau_{A,\lambda'}$ is small on theoretical grounds (Figure 9) and then $\tau_{A,\lambda} - \tau_{A,\lambda'}$ is very nearly $\tau_{A,\lambda}$. This works better for large values of τ than for small values, and also better for haze C than for haze M. This can be improved on by using the wavelength dependence of $\tau_{A,\lambda} - \tau_{A,\lambda'}$ to identify the type of aerosol and use theory then to estimate the absolute size of $\tau_{A,\lambda}$ from the size of the wavelength variations. Of course, one must be careful to measure over a wavelength range in which significant variations of τ_{λ} can be expected for those aerosols which one is attempting to detect.

Near-Infrared Measurements of Molecular Band Absorption

In discussing this region of the spectrum we shall assume a near-vertical viewing geometry and a geosynchronous platform, as before. From the results displayed in Figure 21 we may make the following approximations

$$S_{2R} = S_3 = B = 0 \tag{45}$$

for $.6\mu \leq \lambda \leq 2.5\mu$. Making the previously discussed background subtraction measurements at two different wavelengths (both in the infrared region) we have

$$\frac{1}{F}\left(N_1 - \frac{1}{f(1,2)} N_2\right) = T_s T_{2as} S_{2A} \times T_{2s} T_{2a} R \tag{46}$$

$$\frac{1}{F'}\left(N'_1 - \frac{1}{f(1,2)} N'_2\right) = T'_s T'_{2as} S'_{2A} \times T'_{2s} T'_{2a} R' \tag{47}$$

where we have assumed

$$R^{(2)} = R^{(2)'} = 0 \tag{48}$$

$$S_{2A}^{(2)} = S_{2A}^{(2)'} = 0 \tag{49}$$

$$T_{as}^{(2)} S_1^{(2)} = f(1,2)\, T_{as} S_1 \tag{50}$$

$$T_{as}^{(2)'} S_1^{(2)'} = f'(1,2)\, T'_{as} S_1', \tag{51}$$

and also a reasonably accurate knowledge of f and f'.

We shall now consider the problem of using the set of measurements (43) and (44), to determine the absorption at the center of molecular band, specified by λ'. We shall assume that T_{2a} and T_{2as} are both unity at the reference wavelength λ. Furthermore, since the forward scattered radiation traverses nearly the same atmospheric path as the unscattered radiation, we may assume that $T'_{2a} = T'_{2as}$. Under these assumptions and conditions, (43) and (44) become

$$X = T_s^2 R + T_s S_{2A} \tag{52}$$

$$X' = T'_{2a}(T_s^{2'} R' + T'_s S'_{2A}) \tag{53}$$

where X and X' are the left-hand sides of (43) and (44), respectively. Solving this system for the absorption at wavelength λ' we have

$$A_{2,\lambda'} = 1 - T'_{2a} = \frac{\left[\frac{T_s^{2'}}{T_s^2} X - X'\right] - \frac{T'_s}{T_s}[T_s S'_{2A} - T'_s S_{2A}]}{\frac{T_s^{2'}}{T_s^2} X + \frac{T'_s}{T_s}[T_s S'_{2A} - T'_s S_{2A}]} \tag{54}$$

where the subscript (2) on $A_{2,\lambda'}$ refers to the double traversal of the atmosphere. Let us assume at this point that Rayleigh scattering is negligible in influencing T_s and T'_s. In most cases in the infrared the aerosol sky glint component $T_s S'_{2A} - T'_s S_{2A}$ may be neglected relative to either X or X' (Figure 22). However, the difference $(T'^2_s/T^2_s)X - X'$ may not be large compared to the sky glint term. This arises when the fractional absorption at λ' is small compared to one. The smallest absorption that can be measured thus depends upon the size of the scattered background and on how well it can be estimated. For the case in which λ is very close to λ' and $T_s/T'_s \approx 1$, Eq. (51) takes the simpler form

$$A_{2,\lambda'} = \frac{X - X'}{X}. \tag{55}$$

For $\lambda = 1.0\mu$, $\lambda' = .94\mu$ and with $f(1,2)$ accurate to 10%, we find that the absorption (due to water vapor in this case) for a double traversal of the atmosphere is related to the quantities X and X' by

$$A_{2,\lambda'} = \frac{X - X'}{X} - .009\frac{X'}{X} \pm .015 . \qquad (56)$$

Thus we could use (52) without a significant loss of accuracy and obtain the water vapor absorption to within approximately .02, which is an adequate sensitivity to be useful (changes greater than .25 precipitable cm. could be observed with a spectrometer of .03μ resolution). It appears that water vapor absorption measurements from a satellite using the sun glint are easily feasible.

Calibration at 4μ

We have already noted that the sun glint and earth's black body spectral radiances are comparable near $\lambda = 4\mu$. It has been suggested that since this region is also an atmospheric window, a measure of the sea surface temperature (which determines B) could be used to calibrate the sun glint (McClintock, 1970).[1] Measurements of B ($\lambda = 10\mu$) from a satellite can be used to infer B ($\lambda = 4\mu$) through Planck's equation. At $\lambda = 4\mu$ equations (22) and (24) reduce to

$$N_1 = [T_{as}S_{1A} + T_s T_{2as} S_{2A} + T_{2s}T_{2A}(S_4 + R)]F + T_s T_a B \qquad (57)$$

$$N_2 = [T_{as}^{(2)}S_{1A}^{(2)} + T_{2s}^{(2)}T_{2a}^{(2)}S_4^{(2)}]F + T_s^{(2)}T_a^{(2)}B \qquad (58)$$

where we have assumed a geometry such that $R^{(2)} = S_{2A}^{(2)} = 0$, and a sea surface emissivity which is independent of view angle. We may also assume that $T_{2s} = T_s^2$ and $T_{2as} = T_{2a}$, the latter applying best for a near-vertical viewing geometry. Dividing by F we thus have

$$N_1/F = [T_a S_{1A} + T_s T_{2a} S_{2A} + T_s^2 T_{2a}(S_4 + R)] + T_s T_a B/F \qquad (59)$$

$$N_2/F = [T_a^{(2)}S_{1A}^{(2)} + T_s^{(2)2}T_{2a}^{(2)}S_4^{(2)}] + T_s^{(2)}T_a^{(2)}B/F \qquad (60)$$

How we proceed from here depends on the size of the background terms. For $W \leq 2$m/sec and $\tau_A \leq .1$ the background term (in brackets) is less than 1% of the sun glint signal or B/F. In this case, (54) and (55) reduce to

$$X_1 = N_1/F = T_s^2 T_{2a} R + T_s T_a B/F \qquad (61)$$

$$X_2 = N_2/F = T_s^{(2)} T_a^{(2)} B/F \tag{62}$$

Solving this system for R in terms of the known quantities $X_1, X_2, B,$ and F we have

$$R = \frac{[T_s^{(2)} T_a^{(2)}]^2}{T_s^2 T_{2a}} [X_1 - \frac{T_s T_s}{T_s^{(2)} T_a^{(2)}} X_2] \frac{(B/F)^2}{X_2^2} \tag{63}$$

Because of the low wind speed assumed here the sun glint pattern is very small. Thus the viewing geometries 1 and 2 may be taken close enough together to assume $T_s^{(2)} = T_s$ and $T_a^{(2)} = T_a$. Then (60) reduces to

$$R_{\lambda=4\mu} = \frac{T_a^2}{T_{2a}} [X_1 - X_2] \frac{B^2}{X_2^2 F^2} \tag{64}$$

The ratio T_a^2/T_{2a} is a few percent larger than unity and can probably be approximated to within 1%. Assuming all measured quantities are absolutely accurate, our assumptions (required by ignorance) led to an error of approximately one or two percent in the value of R at $\lambda = 4\mu$. While this appears to be usable, a number of practical problems must also be considered:

(1) Sea surface emissivity variations with wavelength may interfere with determination of B ($\lambda = 4\mu$) from B ($\lambda = 10\mu$).

(2) Even without relative emissivity variations the percent error in B ($\lambda = 4\mu$) inferred from B ($\lambda = 10\mu$) is 2.5 times the percent error in B ($\lambda = 10\mu$).

(3) Current uncertainty in the wavelength dependence of $\rho_\lambda(\omega)$ is relatively large in the 4μ region ($\sim$ 5%) (Figure 16) and degrades the accuracy of the calibration at other wavelengths.

Adding to these factors, instrumental limitations may make this method of sun glint calibration completely unworkable. The usefulness of transmission measurements of 5% accuracy (assuming perfect instrumentation) is questionable in itself.

Conclusions

We have attempted to present here a detailed framework of analysis for estimating the feasibility of sun glint experiments, specifically concentrating on the effect of uncertainties in theory on possible determinations of atmospheric transmission and absorption. Accurate evaluation of experiments depends on the particulars in the method and in the instrumentation. We have not dealt with the latter factors in detail in the report.

We have found that the sun glint can be used without absolute calibration to determine the following:

1) changes of aerosol optical thickness with wavelength with an accuracy of approximately .02 to .03 in optical depth from the visible to near $\lambda = 2.5\mu$ wherever atmospheric windows permit.

2) molecular band absorption for a two-way traversal of the atmosphere with an accuracy of approximately .02 in fractional absorption. (This could be very useful in determining precipitable water vapor from satellite.)

We have found that the above determination can probably not be improved by calibrating the sun glint at $\lambda = 4\mu$, since the errors in this calibration are very likely to be too large for the calibration to be useful.

These conclusions are applicable for the observing conditions we have specified as typical. Included in this specification is a wind speed of 5 m/s. For lower wind speeds the accuracies cited will be conservative. For higher wind speeds the suggested determinations will at some point no longer be feasible. Significant variations of viewing geometry and aerosol loading will also modify these conclusions to varying degrees. To describe the effects of all possible variations of the numerous parameters involved in this study would introduce a degree of complexity which would produce, at this point, more confusion than enlightenment. Instead we have examined a small, but very probable, region of the multidimensional space of variations and have concluded that the sun glint shows promise as an experimental tool for the determination of atmospheric transmission and absorption.

REFERENCES

1. McClintock, M., T. A. Hariharan, and A. McLellan IV, "Studies on Techniques for Satellite Surveillance of Global Atmospheric Pollution," annual report to the National Air Pollution Control Administration, UWI-SSEC-GAP-70-001, September 30, 1970.

2. Vonder Haar, T. H., Ph. D. thesis, University of Wisconsin, Madison (1968).

3. Vonder Haar, T. H. and V. E. Suomi, "Satellite Observations of the Earth's Radiation Budget," Science 163, 667 (1969).

4. Flowers, E. C., R. A. McCormick and K. R. Kurfis, "Atmospheric Turbidity over the United States, 1961-1966," J. Appl. Meteor. 8, 955 (1969).

5. Bryson, R. and W. Wendland, Global Effects of Environmental Pollution, Ed. S. Singer, Springer-Verlag, pp. 130-138 (1970).

6. Davitaia, F., Trans. Soviet Acad. Sci., Geogr. Ser. No. 2 (1965).

7. Risebrough, R., R. Huggett, J. Griffin and E. Goldberg, Science 159, 3820 (1968).

8. Mitchell, J., Global Effects of Environmental Pollution, Ed. S. Singer, Springer-Verlag, pp. 139-155 (1970).

9. Mitchell, J., Annual N.Y. Acad. Sci. 95, 235 (1961).

10. Manabe, S. and R. Wetherald, J. Atmos. Sci. 24, 241 (1967).

11. Atwater, M. A., Science 170, 64 (1970).

12. McCormick, R. A. and Ludwig, C., Science 156, 1358 (1967).

13. Charlson, R. J. and M. J. Pilat, J. Appl. Meteor. 8, 1001 (1969).

14. Angstrom, A., Tellus 14, 435 (1962).

15. Rasool, S. and S. Schneider, Science 173, 138 (1971).

16. Manson, J. E., in Handbook of Geophysics and Space Environments, S. L. Valley, ed., McGraw-Hill Book Company, New York (1965).

17. Kattawar, G. W. and G. N. Plass, "Influence of Particle Size Distribution on Reflected and Transmitted Light from Clouds," Applied Optics 7, 869 (1968).

18. Plass, G. N. and G. W. Kattawar, "Polarization of the Radiation Reflected and Transmitted by the Earth's Atmosphere," Applied Optics 9, 1122 (1970).

19. Deirmendjian, D., "Scattering and Polarization Properties of Water Clouds and Hazes in the Visible and Infrared," Applied Optics 3, 187 (1964).

20. Elterman, L., in Handbook of Geophysics and Space Environments, ed. S. L. Valley, McGraw-Hill Book Company, New York (1965).

21. Cox, Charles C. and Walter Munk, "Measurement of the Roughness of the Sea Surface from Photographs of the Sun's Glitter," J. Opt. Soc. Am. 44, 838 (1954).

22. Levanon, N., "Determination of the Sea Surface Slope Distribution and Wind Velocity Using Sun Glitter Viewed from a Synchronous Satellite," Meteorological Satellite Instrumentation and Data Processing, Final Scientific Report on NASw-65 (1968).

23. Kornfield, J., Ph. D. thesis, University of Wisconsin, Madison, unpublished (1971).

24. Friedman, D., "Infrared Characteristics of Ocean Water (1.5 - 15μ)," Applied Optics 8, 2073 (1969).

25. Coulson, Dave and Sekera, Tables Related to Radiation Emerging from a Planetary Atmosphere with Rayleigh Scattering, Univ. of California Press (1960).

26. Volz, F. E., "Spectral Skylight and Solar Radiance Measurements in the Caribbean: Maritime Aerosols and Sahara Dust," J. Atmos Sci. 27, 1041 (1970).

27. Quenzel, H., "Determination of Size Distribution of Atmospheric Aerosol Particles from Spectral Solar Radiation Measurements," J. Geophys. Res. 75, 2915 (1970).

28. Plass, G. N. and G. W. Kattawar, "Radiative Transfer in an Atmosphere-Ocean System," Applied Optics 8, 455 (1969).

29. Duntley, S. Q. and C. F. Edgerton, The Use of Meteorological Satellite Photographs for the Measurement of Sea State, U. S. Navy, Bureau of Ships, Project FAMOS, Contract NObs-86012 Lot 11, Final Report No. 11-2 (1966).